UNIWERSYTET TECHNOLOGICZNO-PRZYRODNICZY
IM. JANA I JĘDRZEJA ŚNIADECKICH
W BYDGOSZCZY

WYDZIAŁ TELEKOMUNIKACJI
I ELEKTROTECHNIKI

ZESZYTY NAUKOWE NR 257

ELEKTROTECHNIKA
15

BYDGOSZCZ – 2010

UNIWERSYTET TECHNOLOGICZNO-PRZYRODNICZY
IM. JANA I JĘDRZEJA ŚNIADECKICH
W BYDGOSZCZY

ZESZYTY NAUKOWE NR 257

ELEKTROTECHNIKA

15

BYDGOSZCZ – 2010

REDAKTOR NACZELNY
prof. dr hab. inż. Janusz Prusiński

REDAKTOR DZIAŁOWY
dr inż. Sławomir Cieślik

OPRACOWANIE TECHNICZNE
mgr inż. Daniel Morzyński

ISSN 0209-0570

Wydawnictwa Uczelniane Uniwersytetu Technologiczno-Przyrodniczego
ul. Ks. A. Kordeckiego 20, 85-225 Bydgoszcz, tel. 52 3749482, 3749426
e-mail: wydawucz@utp.edu.pl http://www.wu.utp.edu.pl

Wyd. I. Nakład 80 egz. Ark. aut. 4,0. Ark. druk. 4,6.
Zakład Małej Poligrafii UTP Bydgoszcz, ul. Ks. A. Kordeckiego 20

Contents

UNIWERSYTET TECHNOLOGICZNO-PRZYRODNICZY
IM. JANA I JĘDRZEJA ŚNIADECKICH W BYDGOSZCZY
ZESZYTY NAUKOWE NR 257
ELEKTROTECHNIKA 15 (2010) 5-24

AN ANALYSIS OF THE APPLICATIBLITY OF "HOT-POTATO" ROUTING IN WIRELESS SENSOR NETWORKS USED IN ENERGY CONSUMPTION MONITORING SYSTEMS

Bożydar Dubalski[1], Piotr Kiedrowski[1], Jens M. Pedersen[2]

[1]Institute of Telecommunication
University of Technology and Life Sciences
Kaliskiego 7, 85-789 Bydgoszcz, Poland

[2]Department of Electronic Systems
Aalborg University
Fredrik Bajers Vej 7, DK-9220 Aalborg Øst, Denmark

Summary: The subject of this paper is analysis of possibility of application "Hot--Potato" protocol in the Wireless Sensor Networks (WSN), which can be used to collect, store and process data obtained from the media consumption meters. Authors propose to use this protocol on account of its low energy emission and small memory capacity while ensuring the high reliability. To perform this analysis the elements of graph theory were used.

Keywords: WSN, Hot Potato protocol, graph, spanning tree, adjacent matrix, diameter, average path length

1. INTRODUCTION

Dynamic development in the field of wireless transmission technology has aroused interest in building sensor networks. A wireless sensor network (WSN) consists of many cheap and small-sized energy efficient devices, located over a certain area in order to accomplish a common task [6, 10]. These networks can perform a variety of functions connected with monitoring of different objects, collecting data from recording devices; they can also be used in industry as well as for collecting media consumption data by companies supplying users with electricity, gas or water. In the last case, application of the above mentioned technology enables automatic, remote reading of a medium consumption by a user, which not only reduces employment costs but also provides users with service and comfort (no need to wait for the collector, improvement in the security thanks to elimination of the risk of being intruded by unauthorized persons).

The basic element of a sensor network is a node consisting of a sensor monitoring the medium consumption, including processor with limited computing possibilities and a battery or an external power supply (the node is assumed to take a small amount of energy). Another task, apart from the main one which involves data recording, is to transmit it over the radio path to a given node (acquisition center) and also, if necessary, transmit information coming from/to other nodes.

A typical node of WSN consists of an antenna, a microcontroller, a transmission – reception system and a sensor. Nodes of different networks can vary considerably from each other (it results from a variety of tasks to perform); however it is possible to distinguish some elements they have in common. These elements are: measurement module, calculation module, transmission module, supply module and operational system. The task of the measurement module is to collect information gathered by the node. The measurement results, in a digital form (analogue signal is converted into digital one), are transmitted to the calculation module where they are transformed. The calculation model consists of a microcontroller or microprocessor with memory and plays the most important role in cooperation with microprocessors. The transmission module receives and transmits information between the network nodes. The operational system, being the processor central part, manages and controls all the above mentioned modules, enables data transmission between them and monitors their operation.

Most frequently, one module of the sensor network is distinguished and it constitutes the acquisition center. Its task is collecting, storing and processing information coming from each of the sensors belonging to the network. The node equipment is much more developed and the processor possibilities are significantly better than those of the standard node.

Two main features of sensor networks are: connectivity and coverage [11]. Connectivity means the ability of data transmission between all nodes of the network on the condition that it is being able to provide possibilities to transmit information between adjacent nodes (which results from low radio powers generated by sensors), whereas coverage means capability of gathering information from the assigned area.

While building a sensor network it is necessary to account for factors that have a significant influence on the design process and later on its operation. These include:

- Fault tolerance. Some nodes of a sensor network can be unfit for use due to lack of energy, physical contamination, or environmental impact. However, such a situation should not affect accomplishment of the network basic task.
- Scalability. A sensor network can consist of hundreds or even thousands of sensor nodes. For this reason, applications must be designed in such a way that they will be able to operate with a big and variable amount of nodes.
- Production costs. As it has already been mentioned, sensor networks are most often made up of a large number of nodes, thus the cost of a single node has a big influence on the total cost of the whole enterprise.
- Work environment. Sensor networks can operate in various, sometimes extreme, conditions, therefore, the nodes are required to meet very high standards connected with resistance to interference and disruption by external factors.
- Transmission medium. Most frequently communication between nodes is carried out by means of radio waves, though transmission using infrared radiation or optical medium is applied as well.
- Power consumption. In sensor networks using a wireless medium the power intake is of great importance. Sensor nodes are based on microelectronic subsystems must be equipped with a source of electrical energy of limited power since in many cases there is no possibility of its frequent exchange, therefore, the battery life time largely limits costs and efficiency of the whole network. In multi-hop networks where information is transmitted by many nodes, this is the node which is the information source and receiver, and it performs the function of a router. The node turning off or damaging causes the network topology change and involves the necessity of

introduction of new routings, that is, reorganization of the whole network operation. Energy efficiency and its appropriate management need to be accounted for as soon as in the stage of the network design. Thus, energy efficient solutions for subsystems, protocols and algorithms are being continuously searched for.

Recently, many communication protocols have been elaborated for WSN networks, where the basic assumption for their design is to solve the problem of a long-term node feed [10]. In typical networks, the choice of the route is made in such a way that it is possible to transmit information with possibly smallest total emitted energy with intermediate nodes being uniformly loaded by energy, over the whole time of the network operation. In WSN networks used for building energy consumption monitoring systems, the energy efficiency problem does not appear in most cases. Therefore, in such systems energy inefficient (with high energy consumption), simple routing protocols can be used, e.g. protocols of the type 'Multi-hop by Flooding'.

Acceptance of this kind of solution has two advantages – it provides highly reliable transmission involving possibility of simultaneous transmission of packets through different routes and makes it possible to reduce requirements concerning the capacity of memory installed in the sensor node. The advantage is of special importance as in systems of remote readings it is necessary to have increasingly higher capacity for implementation of more and more complicated coding algorithms. Additionally, the biggest part of memory RAM has to be designed for transmission-reception buffers which are the effect of transmission of packets with increasing length that must be handled by WSN networks.

Despite the advantages there is a certain drawback of protocols of the type 'Multi-hop by Flooding' which, in combination with the assumption of a wider application of the discussed network, limits its use possibilities. This drawback is its high protocol emissivity amounted w - 1 for a network containing w number of nodes.

For this reason, the authors of the paper focus on an analysis of possibilities of using 'Hot-Potato' (HP) protocol. Advantages of this protocol are reflected by its below mentioned features:

- It is a reliable protocol as in the process of choosing neighbors, the node chooses only those adjacent nodes which ensure small probability of information transfer error occurrence;
- Despite redundant number of hops, HP protocol is of low emission character because:
  - It is a connectionless protocol (path does not need to be formed);
  - In a given moment, only one node of the whole network can be in the state of transmission;
  - Alternative routes are not set up (as it is done, e.g. in Multipath–Based Routing).
- It needs relatively small capacity of RAM memory as package buffering is not required, and there is no need to know the whole network topology and memory has only the list of neighbors recorded.
- Packages are transferred fast as during the package transfer, delay time is not required;
- Does not require complicated, fast and highly developed equipment;
- Is of non-collision character.

Routing "Hot-Potato" protocol was described for the first time in 1964 in [2]. It found wide application no sooner than in the second half of the 90s, mostly in fast fiber networks [1, 3, 4, 5, 7, 13, 14] where it is better to transmit a packet by fast links through a bigger number of nodes, than to waste time for their buffering, until the optimal route becomes available. For this reason, this protocol is frequently called a deflective protocol. In the solution the node does not know the optimal route, therefore there cannot by any deflection from the optimal route, it is why it is preferred to call this protocol "Hot-Potato" instead deflective protocol. The authors of this paper have not found many publications on the subject of "Hot-Potato" protocol application in systems of wireless communication, and it appears that in WSN networks with relatively fast links (from several to several hundred kb/s) and nodes with poor memory, this protocol can successfully be used.

The subject of this article is an analysis of applicability of elements of graph theory for the design of sensor networks based on "Hot-Potato" protocol. The main contribution of the paper is the demonstration of probability of packet delivery. First a theoretical analysis is presented, based on graph theoretical concepts, and applied to a concrete example. Next the theoretical analysis is confirmed through simulations.

2. PURPOSE OF THE ANALYSIS AND METHODS

The subject of the presented analysis is a specific sensor network designed for a remote reading of media consumption by individual users. This kind of network, as any other one, can be described by means of a graph. Each graph, in turn, can be described by their adjacency matrix [AM] [8], that is a matrix which defines mutual incidence of the graph nodes [12]. This matrix is a square one of w x w dimension (where w denotes the number of nodes forming this network) with elements am_{ij} which assume values from set {0, 1}, whereas:

- $am_{ij} = 1$, when there exists an edge connecting nodes w_i and w_j .
- $am_{ij} = 0$, when there no exists an edge connecting nodes w_i and w_j.

To illustrate the presented considerations, a simple example of a network shown in fig. 1, has been used.

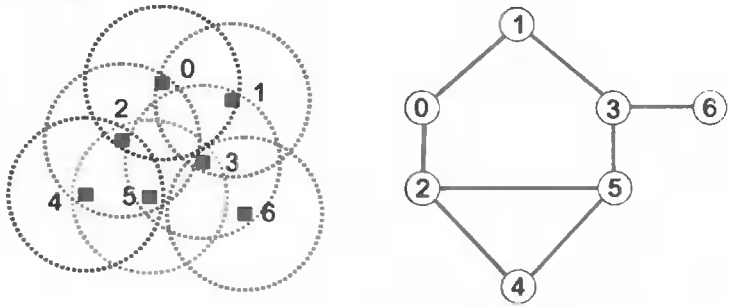

Fig.1. An example scheme of a sensor network and a graph describing it – circles define the range of radio transmission.

The analyzed network consists of 7 nodes and is described by the following adjacency matrix:

$$[AM]=\begin{bmatrix}0&1&1&0&0&0&0\\1&0&0&1&0&0&0\\1&0&0&0&1&1&0\\0&1&0&0&0&1&1\\0&0&1&0&0&1&0\\0&0&1&1&1&0&0\\0&0&0&1&0&0&0\end{bmatrix}$$

The exponentiation of adjacency matrix allows to calculate the number of routes with length ***l*** which connect two random vertices of the graph (a route is an alternate series of nodes and edges in which each node and each edge can appear many times and the number of edges forming a given route defines its length [9]). Thus, the number of routes with length 2 is defined by the second power of matrixes **[AM]²**, **[AM]³** – number of routes with length 3, and so on.

$$[AM]^2=\begin{bmatrix}2&0&0&1&1&1&0\\0&2&1&0&0&1&1\\0&1&3&1&1&1&0\\1&0&1&3&1&0&0\\1&0&1&1&2&1&0\\1&1&1&0&1&3&1\\0&1&0&0&0&1&1\end{bmatrix}\quad [AM]^3=\begin{bmatrix}0&3&4&1&1&2&1\\3&0&1&4&2&1&0\\4&1&2&2&4&5&1\\1&4&2&0&1&5&3\\1&2&4&1&2&4&1\\2&1&5&5&4&2&0\\1&0&1&3&1&0&0\end{bmatrix}$$

$$[AM]^4=\begin{bmatrix}7&1&3&6&6&6&1\\1&7&6&1&2&7&4\\3&6&13&7&7&8&2\\6&1&7&12&7&3&0\\6&2&7&7&8&7&1\\6&7&8&3&7&14&5\\1&4&2&0&1&5&3\end{bmatrix}$$

The obtained calculation results provide a lot of useful information.

- Each matrix row defines the number of routes with length *l*, connecting the node with the number corresponding to the row number, with the remaining nodes (also with itself).
- If the matrix element $\boldsymbol{am_{ij}}$, for the first time, assumes value different from zero for the matrix power equal to ***l***, it means that the minimum length of the path linking the ***i***-th node with the ***j***-th one is ***l***.
- On the basis of obtained results it is possible to determine the graph diameter and the average path length.

Diameter of a coherent graph is the distance between two most distant vertices of the graph, that is, the smallest number ***n*** such that two randomly chosen vertices are connected by a path consisting of maximum ***n*** edges. The diameter is defined by the expression:

$$d(G) = \max_{v_i v_j} \{d_{\min}(v_i, v_j)\} . \tag{1}$$

The average path length of the graph is defined as the average number of the graph edges connected by any two nodes and is described in the following way:

$$d_{av} = \frac{1}{w(w-1)} \sum_{i=0}^{w-1} \sum_{j=0}^{w-1} d_{\min}(v_i, v_j) \tag{2}$$

- The sum of all elements occurring in a given row of the matrix is a general number of routes of given lengths that can occur in the analyzed network if a node with the number corresponding to this row is accepted as the source node.
- The sum of all elements occurring in the matrix defines the overall number of routes of given lengths occurring throughout the analyzed network.

In order to simplify and shorten the calculation process (through avoiding the matrix raising to power) it is possible to use repeated multiplying of vector $[V_i]$ describing connections between a chosen source node and the remaining ones, that is, the row corresponding to this node through matrix **[AM]**, that is:

$$\begin{aligned} [Vi]^2 &= [Vi]^1 [AM] \\ [Vi]^3 &= [Vi]^2 [AM] \\ &\ldots \\ &\ldots \\ [Vi]^j &= [Vi]^{j-1} [AM] \end{aligned} \tag{3}$$

where: ***j*** denotes the route length.

In the analyzed example, shown in fig, 1, vectors describing distributions of routes with lengths 1 to 8, for the source node with number 3, have the form:

$$[V_3]^1 = [0, 1, 0, 0, 0, 1, 1]$$
$$[V_3]^2 = [1, 0, 1, 3, 1, 0, 0]$$
$$[V_3]^3 = [1, 4, 2, 0, 1, 5, 3]$$
$$[V_3]^4 = [6, 1, 7, 3, 12, 7, 3]$$
$$[V_3]^5 = [8, 18, 16, 4, 10, 26, 12]$$
$$[V_3]^6 = [34, 12, 44, 56, 42, 30, 4]$$
$$[V_3]^7 = [56, 90, 106, 46, 74, 142, 56]$$
$$[V_3]^8 = [196, 102, 272, 288, 248, 226, 46]$$

Applying the above observations to the example network, shown in fig.1, it can be said that:

- Accepting an assumption that the node with number 0 is a source node and the length of routes is 3, then table 1 describing a set of these routes to destination nodes has the form:
- Minimal length of the path connecting number 0 node with nodel is 1, with node 2-1, node 3-2, node 4-2, node 5- 2, node 6 – 3, thus, the diameter of graph describing this network is 3.

Table 1. Set of routes to destination nodes

Destination node number							Sum of routes
0	1	2	3	4	5	6	
0	3	4	1	1	2	1	12
Number of routes							

- Average lengths of paths hale been presented in table 2, depending on the accepted source node.

Table 2. Average length of paths

Source node	Average length of paths
0	1,833
1	1,833
2	1,667
3	**1,500**
4	2,000
5	**1,500**
6	2,333

The considered method can be applied in the searching for nodes being roots of minimal spanning trees describing the designed network.

A tree is called a rooted tree if one vertex has been designated as the root. In a rooted tree there is exactly one path between a randomly chosen node and the root. The number of edges in a path his called length, a number with one value higher defines the node level, and the tree height is the highest level existing in a given tree.

To illustrate this, in table 3, there have been given heights of created trees, depending on the choice of the node number, selected as the tree root.

Table 3. Height of spanning trees

Source node	Height of spanning trees
0	3
1	3
2	3
3	**2**
4	3
5	**2**
6	3

The above presented table shows that the tree root should be in node 3 or 5.

In table 4 and in fig. 2 a summary comparison of the number of routes calculated for successively chosen nodes has been given, neglecting routes which form their own loops.

On the basis of received results it can be concluded that the maximum number of routes connecting a chosen node with the other ones, in the possession of node number 5, thus, this node should be selected as the acquisition node location.

With the assumption that this node is a source node, the calculated average length of paths is minimal just as the height of the spanning tree. However, the summary number of bypass routes is maximal which causes an increased probability that the information will reach its address.

Table 4. Summary lengths of routes

Source node	Length of route					
	1	2	3	4	5	6
0	2	3	12	23	70	152
1	2	3	11	21	64	137
2	3	4	17	33	100	223
3	3	6	16	36	94	222
4	2	4	13	30	82	195
5	**3**	**5**	**17**	**36**	**102**	**233**
6	1	2	6	13	36	82
	Sum number of router					

The considered example is not complicated and benefits from optima choice of location for the acquisition node is insignificant, however, in wide networks, consisting of hundreds nodes, the location of this distinguished node can be important. It will have an influence on the time of packets presence in the network and thereby, on the total time of data collection and error rate. This is of importance in case of 'Hot-potato' algorithm application for information transmission and reception.

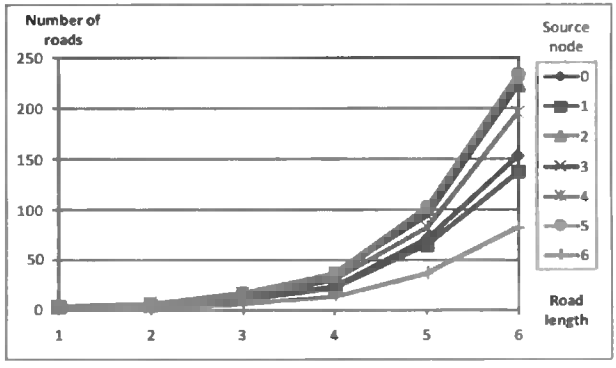

Fig. 2. Summary distribution of router depending on the accepted source node

3. ANALYSIS OF PROBABILITIES

The above presented network analysis has been used for determination of probability for the information to reach its destination node from the source node with a defined route length assumed. The coefficient defining this probability has been calculated by dividing the vector element specifying the number of routes corresponding to the chosen node by a summary number of routes with given lengths.

$$p_{ri}(m) = \frac{r_i}{\sum_{i=0}^{n-1} r_{ri}} \tag{4}$$

where:

$p_{ri}(m)$ – probability of reaching the i-th node by information, after having covered the m edge of graph,

r_i – number of routes connected source node and chosen node with length m.

Referring to the considered example, the results shown in table 5 and fig. 3 have been obtained for source node number 3.

Table 5. Probability of reaching a given node depending on the route length

Route length	Destination node						
	0	1	2	3	4	5	6
1	0,000	0,333	0,000	0,000	0,000	0,333	0,333
2	0,167	0,000	0,167	0,500	0,167	0,000	0,000
3	0,063	0,250	0,125	0,000	0,063	0,313	0,188
4	0,167	0,028	0,194	0,333	0,194	0,083	0,000
5	0,085	0,191	0,170	0,043	0,106	0,277	0,128
6	0,153	0,054	0,198	0,252	0,189	0,135	0,018
7	0,098	0,158	0,186	0,081	0,130	0,249	0,098
8	0,142	0,074	0,197	0,209	0,180	0,164	0,033
9	0,107	0,138	0,192	0,107	0,142	0,231	0,082
10	0,135	0,087	0,196	0,185	0,173	0,180	0,044
	Probability						

The presented chart proves that if the route length exceeds value 20 which corresponds to the time period of the packet presence in the network, the probability of reaching particular nodes by the information does not change, in fact. Anyway, if node 3 is the source one, then the probability of reaching node 0 by the information is 0.12, 1 – 0.11, 2 – 0.195, 3 – 0.15, 4 – 0.16, 5 – 0.2, whereas, for node 6 – 0.06. This means that if the packet transferred to a given node will stay in the network for time corresponding to the time needed for covering the distance of ***m*** hops, then it should reach its destination with probability pre-determined by the above discussed method.

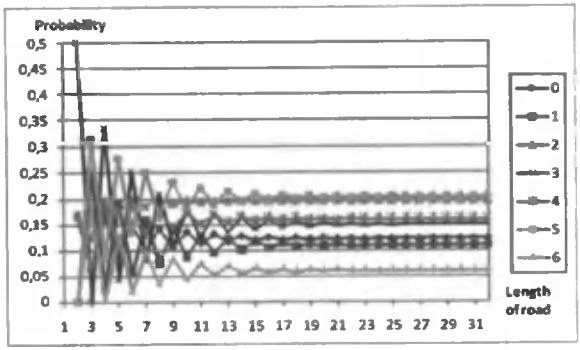

Fig. 3. Probability of reaching a given node depending on the route length

Probability that the packet will reach a given node can also be defined in a different way by creating probability matrix $[AM_p]$, describing probability of choosing a given node as the destination one for data transmission.

With reference to the considered example this matrix will have the form:

$$[AM_p]=\begin{bmatrix} 0.000 & 0.500 & 0.500 & 0.000 & 0.000 & 0.000 & 0.000 \\ 0.500 & 0.000 & 0.000 & 0.500 & 0.000 & 0.000 & 0.000 \\ 0.333 & 0.000 & 0.000 & 0.000 & 0.333 & 0.333 & 0.000 \\ 0.000 & 0.333 & 0.000 & 0.000 & 0.000 & 0.333 & 0.333 \\ 0.000 & 0.000 & 0.500 & 0.000 & 0.000 & 0.500 & 0.000 \\ 0.000 & 0.000 & 0.333 & 0.333 & 0.333 & 0.000 & 0.000 \\ 0.000 & 0.000 & 0.000 & 1.000 & 0.000 & 0.000 & 0.000 \end{bmatrix}$$

Values of the matrix given elements result from an analysis of the exemplary network which has been shown in fig. 4.

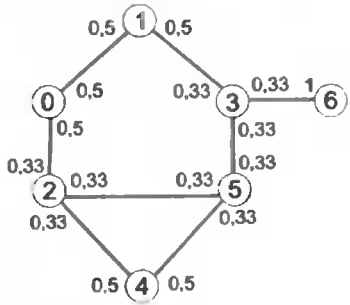

Fig. 4. Distribution of path choice probabilities

Using basic operations to be performed on matrixes it is possible to determine the probability of reaching the destination node by a packet transmitted by a randomly chosen acquisition node, for set time of the packet presence in the network (this time corresponds to the number of hops as this packets has to travel between the source and the destination nodes).

Table 6. Probability of reaching destination by the packet sent by a given acquisition node

Hops number	Number of destination node						
	0	1	2	3	4	5	6
1	0.000	0.333	0.000	0.000	0.000	0.333	0.333
2	0.167	0.000	0.111	0.611	0.111	0.000	0.000
3	0.037	0.287	0.139	0.000	0.037	0.296	0.204
4	0.190	0.019	0.136	0.446	0.145	0.065	0.000
5	0.055	0.244	0.189	0.031	0.067	0.266	0.149
6	0.185	0.038	0.150	0.359	0.152	0.107	0.010
7	0.069	0.212	0.204	0.065	0.085	0.246	0.120
8	0.174	0.056	0.159	0.308	0.150	0.132	0.022
9	0.081	0.190	0.206	0.094	0.097	0.230	0.103
10	0.163	0.072	0.166	0.274	0.145	0.148	0.031

In order to check the obtained results one can calculate the probability of reaching destination by the packet from node 3 to node 0 by routes with length of 4 hops.

Table 7. Calculations concerning the packet probability of reaching its destination

Route	Probability
3 – 6 – 3 – 1 – 0	$\frac{1}{3}\cdot 1\cdot\frac{1}{3}\cdot\frac{1}{2}=\frac{1}{18}$
3 – 1 – 3 – 1 – 0	$\frac{1}{3}\cdot\frac{1}{2}\cdot\frac{1}{3}\cdot\frac{1}{2}=\frac{1}{36}$
3 – 5 – 3 – 1 – 0	$\frac{1}{3}\cdot\frac{1}{3}\cdot\frac{1}{3}\cdot\frac{1}{2}=\frac{1}{54}$
3 – 1 – 0 – 1 – 0	$\frac{1}{3}\cdot\frac{1}{2}\cdot\frac{1}{2}\cdot\frac{1}{2}=\frac{1}{24}$
3 – 5 – 4 – 2 – 0	$\frac{1}{3}\cdot\frac{1}{3}\cdot\frac{1}{2}\cdot\frac{1}{3}=\frac{1}{54}$
3 – 1 – 0 – 2 – 0	$\frac{1}{3}\cdot\frac{1}{2}\cdot\frac{1}{2}\cdot\frac{1}{3}=\frac{1}{36}$
Result	0.190

The obtained results are similar to the results obtained with the use of the above presented method and it can be said that the quantities of probabilities stabilize after having covered by the packet 20 edges of the graph describing the analyzed network (fig.5).

The so far carried out network analysis has not provided any answer to the question – what is the resultant probability for the transmitted packets to reach the destination node. In order to find the answer probability matrixes were used again introducing the following modification. If the transferred package reaches its destination, its further transmission, regardless of the distance it has covered, does not

make sense, therefore in the row of $[AM_p]_m$ matrix corresponding to the number of the destination node, there are placed zeros, which means that this node will not transmit the received information to other nodes.

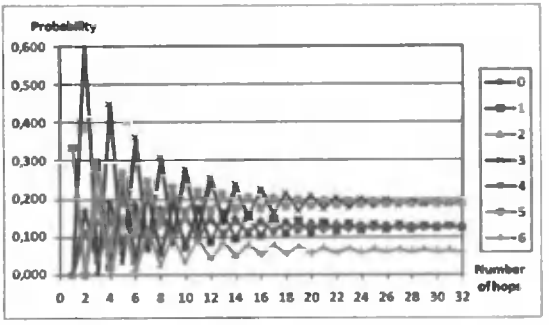

Fig. 5. Distribution of the packet probabilities of reaching its destination nodes

For instance, if the destination node is node 0, then no matter which node is the source one, probability matrix will be of the form:

$$\left[AM_p\right]_m = \begin{bmatrix} 0.000 & 0.000 & 0.000 & 0.000 & 0.000 & 0.000 & 0.000 \\ 0.500 & 0.000 & 0.000 & 0.500 & 0.000 & 0.000 & 0.000 \\ 0.333 & 0.000 & 0.000 & 0.000 & 0.333 & 0.333 & 0.000 \\ 0.000 & 0.333 & 0.000 & 0.000 & 0.000 & 0.333 & 0.333 \\ 0.000 & 0.000 & 0.500 & 0.000 & 0.000 & 0.500 & 0.000 \\ 0.000 & 0.000 & 0.333 & 0.333 & 0.333 & 0.000 & 0.000 \\ 0.000 & 0.000 & 0.000 & 1.000 & 0.000 & 0.000 & 0.000 \end{bmatrix}$$

In fig. 6 the above discussed reasoning has been demonstrated.

Having done multiplication of vectors by matrix $[AM_p]_m$, the distribution of the packet probability to reach a given node was calculated, depending on the distance covered by it which, as it has already been mentioned, will correspond to the time of the packet presence in the network. As compared to the previously analyzed case, the number of possible routes decreases as there will be eliminated those routes for which node with number 0 performed the function of the transit one.

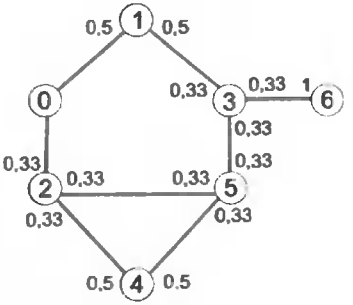

Fig. 6. Distributions of the packet route choice probability

Table 8. Calculation of resultant probability for the packet to reach node 0 from node 3 if the distance length is 4.

Route	Probability
3 – 6 – 3 – 1 – 0	$\frac{1}{3}\cdot 1\cdot\frac{1}{3}\cdot\frac{1}{2}=\frac{1}{18}$
3 – 1 – 3 – 1 – 0	$\frac{1}{3}\cdot\frac{1}{2}\cdot\frac{1}{3}\cdot\frac{1}{2}=\frac{1}{36}$
3 – 5 – 3 – 1 – 0	$\frac{1}{3}\cdot\frac{1}{3}\cdot\frac{1}{3}\cdot\frac{1}{2}=\frac{1}{54}$
3 – 5 – 4 – 2 – 0	$\frac{1}{3}\cdot\frac{1}{3}\cdot\frac{1}{2}\cdot\frac{1}{3}=\frac{1}{54}$
Result	0.120

In the table 9 and the figure 7, the distribution of probability of reaching destination by the packet sent from node 3 to destination node 0 has been shown, depending on the number of hops covered by this packet.

In charts presented in fig. 8, calculated distributions of the packet probability to reach its destination node in the function of the number of hops, have been shown for the case when node 5 which, according to the earlier analysis, should be an acquisition node, is a source node.

Table 9. Distribution of the packet probability to reach its destination depending on the number of hops to cover.

Hops number	Probability	Resultand probability	Hops number	Probability	Resultand probability
1	0.000	0.000	16	0.025	0.816
2	0.167	0.167	17	0.017	0.833
3	0.037	0.204	18	0.019	0.852
4	0.120	0.324	19	0.014	0.866
5	0.039	0.363	20	0.015	0.881
6	0.091	0.454	21	0.011	0.893
7	0.036	0.491	22	0.012	0.905
8	0.069	0.560	23	0.009	0.914
9	0.033	0.593	24	0.010	0.923
10	0.053	0.646	25	0.008	0.931
11	0.028	0.674	26	0.008	0.939
12	0.041	0.715	27	0.006	0.945
13	0.024	0.739	28	0.006	0.951
14	0.032	0.771	29	0.005	0.956
15	0.020	0.791	30	0.005	0.960

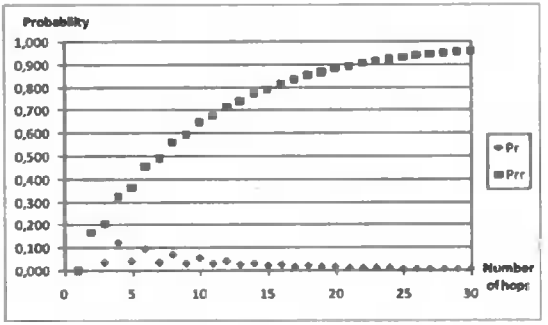

Fig. 7. Chart of the packet probability to reach its destination node, depending on the number of hops. Pr – probability for a given number of hops, Prr – resultant probability.

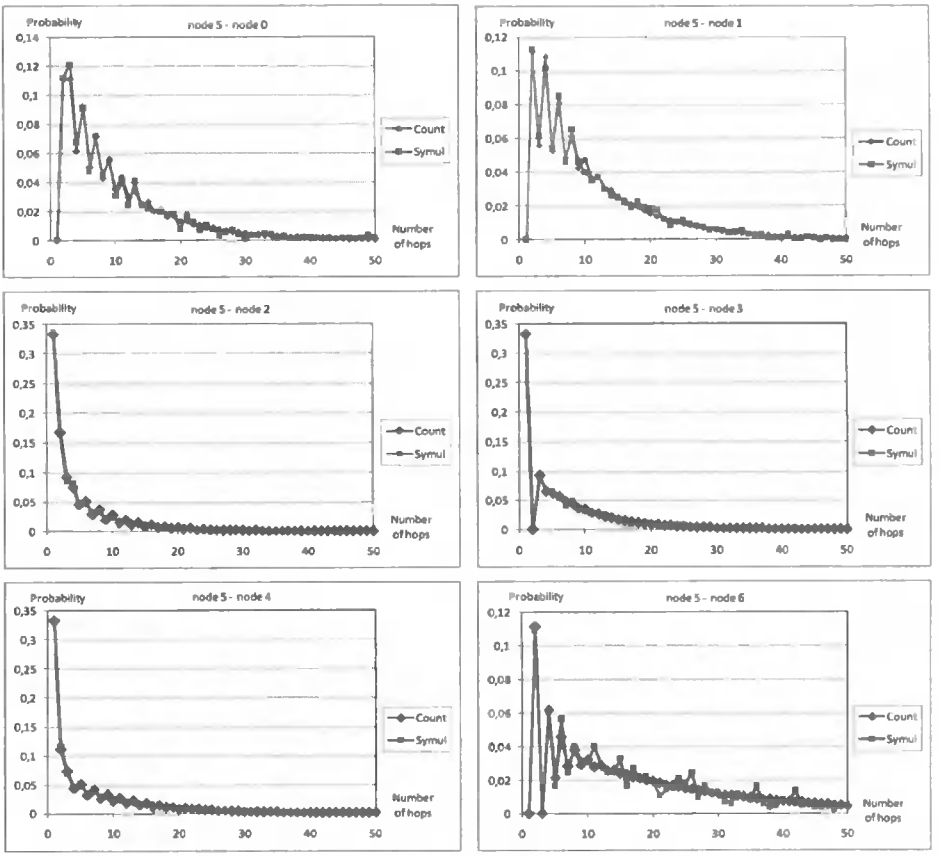

Fig. 8. Distribution of the packet probability to reach its destination node for the case when the destination node is node 5

4. SIMULATIONS

To verify the demonstrated solution to the problem, a computer simulation of a virtual network, shown in fig 1, has been performed, calculating the probability of the packets reaching selected destination nodes, and comparing the obtained results with the theoretically calculated results. In charts (fig.8) the above mentioned distributions obtained from tests performed with the use of a simulation program developed by the authors, have also been given. These tests have proved the rightness of the carried out studies.

Transmission of information takes place in two directions. Reception of the packet by a destination node triggers the process of the return packet transmission which contains information on the node state. Thus, it is also necessary to define the number of hops necessary for transmission of the return information from the destination node to the acquisition one. From the performed calculations it results that the packet, theoretically, should reach the nodes of the analyzed network with probability 0.95 or 0.98 if the number of hops is larger than that, given in table 10.

Table 10. Calculation of the number of hops for which the packet should reach the destination node with the assumed probability

		Source node						
Probability	Destination node	0	1	2	3	4	5	6
0.95	0	-	23	26	28	28	29	29
	1	24	-	30	26	31	30	27
	2	17	20	-	21	13	16	22
	3	23	19	24	-	24	22	1
	4	30	31	25	31	-	25	32
	5	17	18	14	17	11	-	18
	6	65	62	66	56	66	64	-
0.98	0	-	31	34	37	37	37	38
	1	33	-	39	35	40	39	36
	2	23	26	-	27	19	22	28
	3	30	25	31	-	31	29	1
	4	39	40	34	40	-	34	41
	5	22	23	19	21	16	-	22
	6	85	81	86	75	86	84	-

Calculation results and the results obtained in effect of carried out simulations concerning probability of return transmission to node 5, have been demonstrated in figure 9.

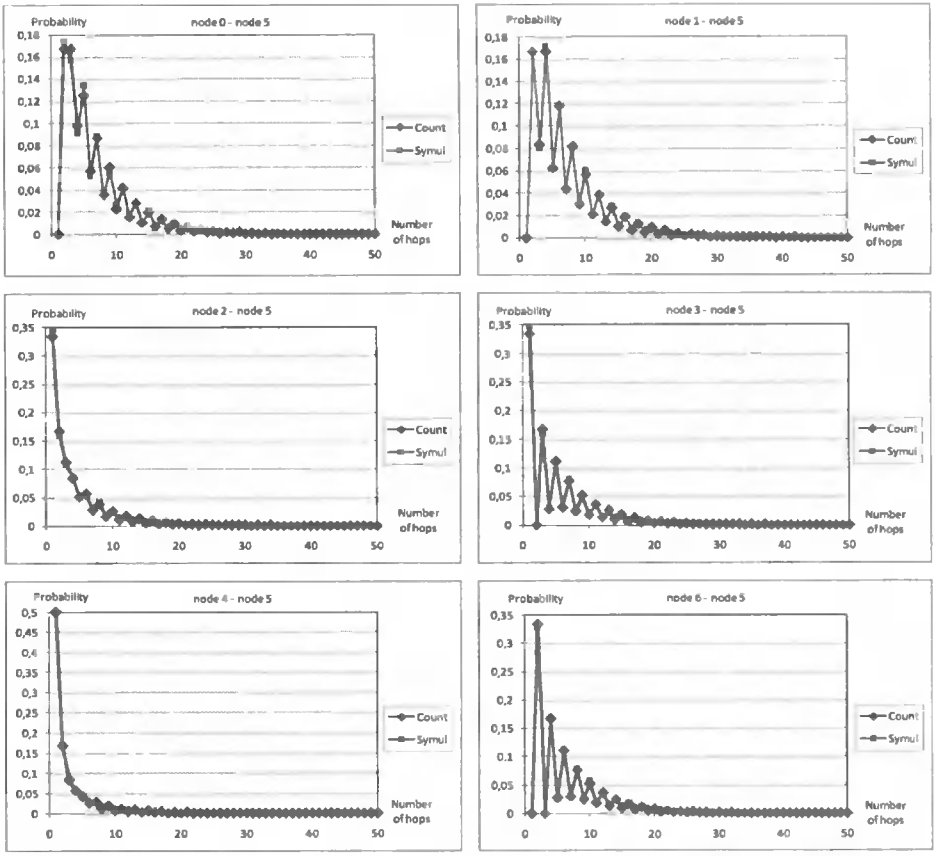

Fig. 9. Distribution of probability for the return packet to reach the destination acquisition node

Summing up the obtained results contained in table 10, the number of hops necessary to transmit and receive a packet to/from nodes has been calculated, with assumed probability of the packet reaching its destination nodes. These results have been included in tables 11 and 12. After having multiplied them by the time needed to transmit the packet to successive nodes, one can calculate time necessary for reception of return information that is, time of waiting for the answer, after which transmission of the next packet will follow.

The obtained results confirm the earlier statement that the optimal location of an acquisition node is node 5 as the total time of the transmitted from this node packet presence, counting from its transmission to its reception, is relatively the shortest.

The main drawback of the 'Hot-Potato' algorithm is lack of certainty whether the packet will reach its destination node. The transmitted packet, apart from the information and control elements, is supplied only with addresses of nodes: source node, transit node and the destination one. This packet can move in the network in both directions "forward" and "backward". In a special case it can oscillate between a certain set of nodes and never reach its destination. To avoid such a situation it is necessary to define the packet life time after which it is removed from the network and another packet should be sent instead. This time, calculated with the use of the considered

method, will be equal to the sum of maximum periods of time of the package presence in the network, for both directions of transmission, with the assumed probability for the return packet to reach the source node.

Table 11. Calculation of the total number of hops for which the packet should come back to the sink node with the assumed probability

Resultant probability	Destination node	Sink node						
		0	1	2	3	4	5	6
0,90	0	0	47	43	51	58	46	94
	1	47	0	50	45	62	48	89
	2	43	50	0	45	38	30	88
	3	51	45	45	0	55	39	57
	4	58	62	38	55	0	36	98
	5	46	48	30	39	36	0	82
	6	94	89	88	57	98	82	0
	Total hops number	339	341	294	292	347	281	508

Table 12. Calculation of the total number of hops after which the transmitted packet should come back to the sink node with the assumed probability

Resultant probability	Destination node	Sink node						
		0	1	2	3	4	5	6
0,96	0	0	64	57	67	76	59	123
	1	64	0	65	60	80	62	117
	2	57	65	0	58	53	41	114
	3	67	60	58	0	71	50	76
	4	76	80	53	71	0	50	127
	5	59	62	41	50	50	0	106
	6	123	117	114	76	127	106	0
	Total hops number	446	448	388	382	457	368	663

There is one more case that should be accounted for, when the transmitted packet will return to the source node before the assumed time designed for information transmission. Then, it is necessary to analyze data included in the received packet. If this information comes from the destination node it means that transmission has been successfully completed and it is possible to go on to examine the successive node. If the received packet was sent by the source node, removal of this packet and its repeated transmission with TTL (Time To Live) value should follow in order to shorten the time of information exchange and increase probability of achieving the effect of positive transmission.

Probability of occurrence of such a situation can be determined by multiplying vectors, describing probability for the information sent from the source node to reach destination nodes, by a modified probability matrix. Summing values of the resultant vector elements, characteristic for the above mentioned nodes, probability of reaching its destination node by the transmitted packet and probability of the packet return to the source node in the function of covered by this packet distance length, can be determined.

For example in table 13, calculated results of the considered probabilities have been shown in the function of the number of hops for nodes 5 (source) and 3 (destination).

Table 13. Distribution of probabilities of reaching destination node by the packet depending on the number of hops

Hops number	Probability of reaching node 3	Probability of return to node 5	Resultant probability
1	0,3333	0,00000	0,33333
2	0,0000	0,27778	0,61111
3	0,0000	0,11111	0,72222
4	0,0278	0,06481	0,81481
5	0,0139	0,03704	0,86574
6	0,0162	0,02623	0,90818
7	0,0081	0,01698	0,93326
8	0,0083	0,01260	0,95415
9	0,0041	0,00836	0,96666
10	0,0042	0,00626	0,97708
11	0,0021	0,00417	0,98333
12	0,0021	0,00313	0,98854
13	0,0010	0,00208	0,99167
14	0,0010	0,00156	0,99427
15	0,0005	0,00104	0,99583
16	0,0005	0,00078	0,99714
17	0,0003	0,00052	0,99792
18	0,0003	0,00039	0,99857
19	0,0001	0,00026	0,99896
20	0,0001	0,00020	0,99928
21	0,0001	0,00013	0,99948
22	0,0001	0,00010	0,99964
23	0,0000	0,00007	0,99974
24	0,0000	0,00005	0,99982
25	0,0000	0,00003	0,99987
26	0,0000	0,00002	0,99991
27	0,0000	0,00002	0,99993
28	0,0000	0,00001	0,99996
29	0,0000	0,00001	0,99997
30	0,0000	0,00001	0,99998
Sum	0,42423	0,57574	

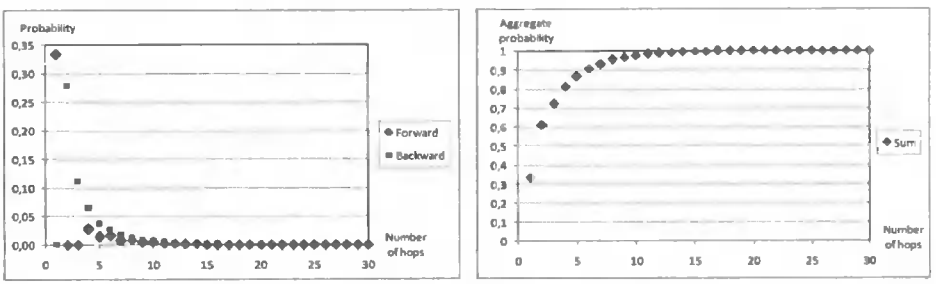

Fig. 10. Charts of the packet probability to reach the destination node (Forward) and its return to the source node (Backward) and resultant probability (Sum) in the function of hop number

In charts presented in fig. 11, calculated distributions of the packet probability to reach the destination and source nodes in the function of hops number, for a case when node 5 is the source node, and accounting for two direction transmission, have been shown.

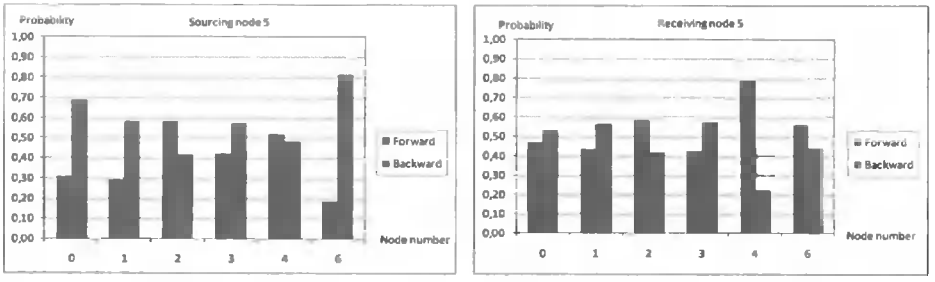

Fig. 11. Distribution of probability to reach by the packet the destination node and its return to the source node versus hop number

The obtained results make it possible to indicate those nodes, sending packets to which will be connected with an assessment of their risk of their return to the transmission node. An analysis of these results can enable an increase in this uncertainty through modification of the network thanks to the rising number of acquisition nodes.

5. CONCLUSIONS

In the paper we have studied the applicability of the "Hot-Potato" protocol in Wireless Sensor Networks, by providing a graph theory based analysis. Two aspects have been focused upon.

First, we have presented a methodology of using adjacency matrixes for calculation of the discussed networks basic parameters – their diameter mean length of paths, and for finding a root of the minimal spanning tree.

This has then been used to study the probability of reaching the destination nodes by transmitted packets and indirect calculation of time for the packets in the network with the assumed probability of a two direction (question-answer) transmission accomplishment.

On the basis of the obtained results it is possible to make a choice of an optimal location for an acquisition node, thanks to which the time of the packet stay in the network will be minimal, which again will shorten the time for data collection, limit emission of radio waves, and minimize the error rate. The carried out theoretical studies, have been verified by using a computer simulation which confirmed the correctness of the considerations.

These studies assume invariable static transmission conditions. Further works in this field will aim at proving usefulness of this analysis in real conditions when the network parameters are not stable, i.e. during transmission of information the links undergo change their parameters, which is connected with reflections, interferences, and wave absorption. It will also be interesting to compare the "Hot-Potato" protocol with other protocols used in Wireless Sensor Networks. Future studies should also address the scalability issues of Wireless Sensor Networks, and include results of much larger networks.

BIBLIOGRAPHY

[1] Acampora A.S., Shah S.I.A., 1992. Multihop Lightwave Networks: A Comparison of Store-and-Forward and Hot-Potato Routing. IEEE Transaction on Communications, Vol. 40, No. 6, pp. 1082-1090.

[2] Baran P., 1964. On Distributed Communication Networks, IEEE Transaction on Communications Syst. Vol. CS-12.
[3] Bononi A., Castanon G.A., Tonguz O.K., 1999. Analysis of Hot-Potato Optical Networks with Wavelength Conversion. Journal of Lightwave Technology, Vol. 17, No. 4, pp. 525-534.
[4] Busch C., Herlihy M., Wattenhofer R., 2001. Routing without Flow Control. Proceedings of the 13th Annual ACM Symposium on Parallel Algorithms and Architectures, Hersonissos, Greece, pp. 11-20.
[5] Caragiannist, Kaklamanis C., Vergadod I., 2000. Greedy Dynamic Hot-Potato Routing on Arrays. IEEE Parallel Architectures, Algorithms and Networks, I-SPAN 2000. Proc. International Symp., pp. 178-185.
[6] Goszczyński T., 2009. Określanie pokrycia bezprzewodowej sieci sensorowej metodą obliczania ścieżki najmniejszej ekspozycji. Pomiary, Automatyka Robotyka 7/8, pp. 9-13.
[7] Gjessing S., 2007. On Burst Loss in Optical Burst Switched Networks with Hot Potato Deflection Routing. IEEE Computer Society, Proc. of the First International Conference on the Digital Society, 2007
[8] Graham R.L., Knuth D.E., Patashnik O., 1994. Concrete Mathematics. Addison-Wesley Comp. Inc.
[9] Korzan B., 1978. Elementy teorii grafów i sieci. Metody i zastosowania. WNT Warszawa.
[10] Mahalik N.P., 2007. Sensor Networks and Configuration. Fundamentals, Standards, Platforms, and Applications, XX, Springer. ISBN: 978-3-540-37364-3.
[11] Ren M., 2009. Bezpieczeństwo komunikacji w sieciach sensorowych. Rozprawa doktorska, UAM Poznań.
[12] Ross K.A., Wright Ch.R.B., 1992. Discrete Mathematics. Prentice Hall Inc.
[13] Szymanski T., 1990. An analysis of `hot-potato' routing in a fiber optic packet switched hypercube. INFOCOM '90. Ninth Annual Joint Conference of the IEEE Computer and Communication Societies. 'The Multiple Facets of Integration'. Proceedings. IEEE, Vol. 3, pp. 918-925.
[14] Zang Z., Acampora A.S., 1994. Performance Analysis of Multihop Lightwave Networks with Hot Potato Routing and Distance-Age-Priorities. IEEE Trans. On Communications Vol. 42, No. 8, pp. 2571-2581.

ANALIZA MOŻLIWOŚCI ZASTOSOWANIA PROTOKOŁU "HOT POTATO" W BEZPRZEWODOWYCH SIECIACH SENSOROWYCH STOSOWANYCH W SYSTEMACH DO MONITOROWANIA ZUŻYCIA ENERGII

Streszczenie

Przedmiotem niniejszego artykułu jest analiza możliwości zastosowania protokołu "Hot-Potato" w bezprzewodowych sieciach sensorowych (WSN), których zadaniem jest zbieranie, przechowywanie i obróbka danych otrzymywanych z liczników monitorujących zużycie mediów. Autorzy proponują zastosowanie tego protokołu ze względu na niską jego emisyjność i niewielką pojemność zastosowanych pamięci przy równoczesnym zachowaniu odpowiedniej niezawodności. W celu dokonania tej analizy wykorzystano elementy teorii grafów.

Słowa kluczowe: bezprzewodowe sieci sensorowe, protokół „Hot Potato", graf, drzewo rozpinające, macierz sąsiedztwa, średnica grafu, średnia długość ścieżki

UNIWERSYTET TECHNOLOGICZNO-PRZYRODNICZY
IM. JANA I JĘDRZEJA ŚNIADECKICH W BYDGOSZCZY
ZESZYTY NAUKOWE NR 257
ELEKTROTECHNIKA 15 (2010) 25-42

ANALYSIS OF THE PARALLEL OPERATION OF THE INDUCTION GENERATORS WITH CAPACITOR EXCITATION

Zdzisław Gientkowski

Zakład Maszyn i Napędów Elektrycznych, Wydział Telekomunikacji
i Elektrotechniki
Al. Prof. Kaliskiego 7, 85-796 Bydgoszcz

Summary: In the paper the parallel operation of the induction generators with capacitor excitation is analysed. The most simple methods of paralleling generators are briefly discussed. A mathematical model for the stationary states of the generators operating in parallel has been presented. The conditions of the best use of the power of the generators operating in parallel have been determined.

Keywords: induction generator, parallel operation, stationary states

1. INTRODUCTION

There are various methods of the paralleling of the induction generators with capacitor excitation [3, 4, 5, 6]. The most appropriate seem to be two methods which with ideal fulfilment of the connection conditions guarantee a surge-free connection process [1, 2, 5, 6].

The first method requires the following conditions to be met:

- the voltage of both generators must be equal,
- voltage frequency must be the same,
- the sequence of phases must be identical.

From all these conditions only the third one is obligatory since if is not met then the state is equivalent to shorting which leads to quick voltage decay and complete demagnetizing of the machine.

As far as the two first conditions are concerned, they do not have to be strictly fulfilled. According to the experimental research carried out by the author, with circa 20 percent voltage and 5 percent frequency difference the transient process of the paralleling of generator lasts for 2 up to 4 periods, and the accompanying current surge does not exceed the quintuple value of the rated current.

The second method does not require any earlier excitation of the generator to be paralleled closed. The process of the synchronization of the second generator runs as follows: first, with the first generator connected to the common busbars a capacitor battery of the generator being synchronized has to be connected. This makes some decrease of frequency and increase of voltage. Since induction generators usually run at a significant saturation of the magnetic circuit, the voltage increase normally is not high. Then, the second generator with its shaft revolving with revolutions close to that of

synchronic is connected (as quickly as possible) to the common busbars. The connection transition process proceeds quickly and with rather small current surges.

The second method is more convenient, however both of them are relatively simple and no intricate instruments are required. Research on transition processes for induction generators running in parallel, including connection to the common power will be discussed in a separate paper.

2. PARALLEL OPERATION OF INDUCTION GENERATORS IN IDLE MODE

At the analysis of the static states of self-excited induction generators it is convenient to use a equivalent circuit of T type where reactive elements are expressed as shown in Fig. 1.

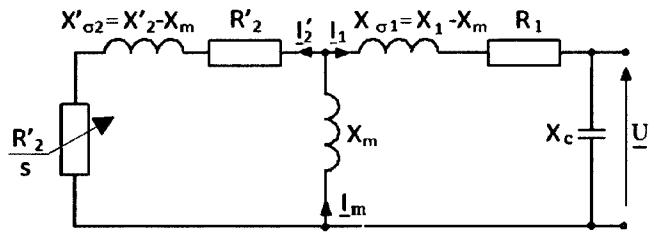

Fig. 1. Equivalent circuit of the induction machine adapted for the considerations (without iron losses)

In the above diagram the reactance X_1 and X_2' represent the total flux linkages of both stator and rotor phases, whereas the reactance X_m the flux linkage of the common inductance. Following relationships are here relevant:

$$\begin{aligned} X_1 &= X_{\sigma 1} + X_m \\ X'_2 &= X'_{\sigma 2} + X_m \end{aligned} \tag{1}$$

where $X_{\sigma 1}$ and $X'_{\sigma 2}$ are leakage reactances of the both stator and rotor windings. Assuming this notation simplifies to a degree the relationships obtained at the analysis.

The system of equations describing the two A and B induction generators in parallel operation in idle mode can be then presented in the form of:

$$\left.\begin{aligned} &(R_{1A} + jX_{1A})\underline{I}_{1A} + jX_{mA}\underline{I}'_{2A} - jX_C\underline{I} = 0 \\ &js_A X_{mA}\underline{I}_{1A} - (R'_{2A} - js_A X'_{2A})\underline{I}'_{2A} = 0 \\ &(R_{1B} + jX_{1B})\underline{I}_{1B} + jX_{mB}\underline{I}'_{2B} - jX_C\underline{I} = 0 \\ &js_B X_{mB}\underline{I}_{1B} - (R'_{2B} - js_B X'_{2B})\underline{I}'_{2B} = 0 \\ &\underline{I}_{1A} + \underline{I}_{1B} - \underline{I} = 0 \end{aligned}\right\} \tag{2}$$

where:

$X_{1A,B}; X'_{2A,B}; R_{1A.B}; R'_{2A,B}; X_{mA}; X_{mB}$ – are the parameters of the equivalent circuit of the A and B induction generators,

$X_C = \frac{1}{\omega_1 (C_A + C_B)}$ – the reactance of the exciting capacitor phase with the assumption that the machine windings are star connected,

$\underline{I} = \underline{I}_C$ – the current in the equivalent circuit (in idle state it equals to the current of one phase of capacitors.

By solving the first and fourth equation of the system of equations (1) with regard to the secondary side and substituting the obtained expressions in the first and forth equation of this system, we obtain:

$$\left.\begin{aligned} &\left[(R_{1A} + jX_{1A}) - \frac{X_{mA}^2 s_A}{R'_{2A} - jX'_{2A} s_A}\right]\underline{I}_{1A} - jX_C \underline{I} = 0 \\ &\left[(R_{1B} + jX_{1B}) - \frac{X_{mB}^2 s_B}{R'_{2B} - jX'_{2B} s_B}\right]\underline{I}_{1B} - jX_C \underline{I} = 0 \\ &\underline{I}_{1A} + \underline{I}_{1B} - \underline{I} = 0 \end{aligned}\right\} \tag{3}$$

After further transformations the system of equations (2) can be presented in the simplified form:

$$\left.\begin{aligned} &\underline{Z}_A \underline{I}_{1A} - jX_C \underline{I} = 0 \\ &\underline{Z}_B \underline{I}_{1B} - jX_C \underline{I} = 0 \\ &\underline{I}_{1A} + \underline{I}_{1B} - \underline{I} = 0 \end{aligned}\right\} \tag{4}$$

where:

$$\left.\begin{aligned} \underline{Z}_A &= R_A + jX_A \\ \underline{Z}_B &= R_B + jX_B \end{aligned}\right\} \tag{5}$$

$\underline{Z}_A$ and $\underline{Z}_B$ components of impedance in equations (5) are determined by formulas:

$$\left.\begin{aligned} R_A &= R_{1A} - \frac{X_{mA}^2 R'_{2A} s_A}{\left(R'_{2A}\right)^2 + \left(X'_{2A} s_A\right)^2} \\ X_A &= X_{1A} - \frac{X_{mA}^2 X'_{2A} s_A^2}{\left(R'_{2A}\right)^2 + \left(X'_{2A} s_A\right)^2} \\ R_B &= R_{1B} - \frac{X_{mB}^2 R'_{2B} s_B}{\left(R'_{2B}\right)^2 + \left(X'_{2B} s_B\right)^2} \\ X_B &= X_{1B} - \frac{X_{mB}^2 X'_{2B} s_B^2}{\left(R'_{2B}\right)^2 + \left(X'_{2B} s_B\right)^2} \end{aligned}\right\} \tag{6}$$

The condition for stable voltage generation in the system composed of two generators running in parallel can be determined from the system of equations (4). The mathematical form of this condition is expressed with the formula:

$$\begin{vmatrix} \underline{Z}_A & 0 & -jX_C \\ 0 & \underline{Z}_B & -jX_C \\ 1 & 1 & -1 \end{vmatrix} = 0 \tag{7}$$

from which we obtain, that:

$$\frac{\underline{Z}_A \underline{Z}_B}{\underline{Z}_A + \underline{Z}_B} = jX_C \tag{8}$$

Taking the left hand side of the equation (8) as a certain substitute $\underline{Z}_z$ impedance we can form the relationship

$$\underline{Z}_z = jX_C \tag{9}$$

which informs that in the system of two induction generators operating in parallel in idle mode the voltage can be generated only when the reactive inductive power necessary for magnetizing of both generators is compensated by the wattless capacitive power of the battery of capacitors of the capacity $C = C_A + C_B$.

The frequency of the voltage generated by the system of two generators can be determined from the equation (8), but it would lead to quite intricate relationships. Much more simple and accurate enough relationship for the frequency of the voltage generated in idle state can be obtained by adopting the following simplifying assumptions:

- slips of the both generators in idle state are equal zero,
- active power losses in the generator system is neglected.

With these assumptions, from (3) we directly obtain, that:

$$\begin{vmatrix} jX_{1A} & 0 & -jX_C \\ 0 & jX_{1B} & -jX_C \\ 1 & 1 & -1 \end{vmatrix} = 0 \tag{10}$$

By substituting

$$X_{1A} = \omega_1 L_{1A}$$
$$X_{1B} = \omega_1 L_{1B}$$

and after the calculation of the (10) determinant we obtain the relationship for the pulsation of the generated voltage ω_1

$$\omega_1 = \frac{1}{\sqrt{\frac{L_{1A} L_{1B} (C_A + C_B)}{L_{1A} + L_{1B}}}} \tag{11}$$

and frequency

$$f_1 = \frac{1}{2\pi\sqrt{\frac{L_{1A}L_{1B}(C_A + C_B)}{L_{1A} + L_{1B}}}} \tag{12}$$

To these expressions the equivalent circuit of the system of the two generators running in parallel in idle state corresponds, and it is presented in Fig. 2a. Designating the equivalent generator inductance as

$$L = \frac{L_{1A}L_{1B}}{L_{1A} + L_{2B}} \tag{13}$$

and its capacity as

$$C = C_A + C_B \tag{14}$$

we obtain the equivalent circuit as in Fig. 2b.

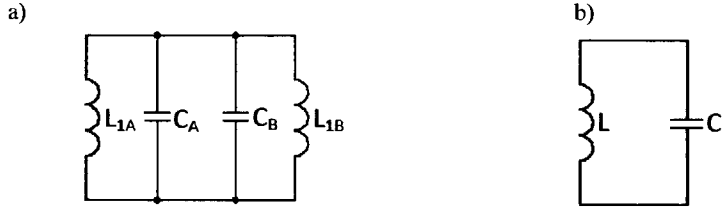

Fig. 2. Equivalent circuit of two induction generators running parallel in idle state – a), and equivalent circuit of generator – b), (L_{1A}, L_{1B} - self-inductances of the phases of the stator of generators A and B, respectively)

Now, the frequency of the voltage generated within the system of two generators operating in parallel in idle mode can be presented with the following, simple relationship

$$f_1 = \frac{1}{2\pi\sqrt{LC}} \tag{15}$$

where:

L – the total inductance of the equivalent generator phase, determined by (13),
C the capacity of one equivalent generator phase, determined by (14).

In order to obtain a equivalent circuit for two self-excited induction generators running in idle mode with commonly used parameters, in equations (2) the substitutes:

$$\left.\begin{aligned} X_{1A} &= X_{1\sigma A} + X_{mA} \\ X'_{2A} &= X'_{2\sigma A} + X_{mA} \\ X_{1B} &= X_{1\sigma B} + X_{mB} \\ X'_{2B} &= X'_{2\sigma B} + X_{mB} \end{aligned}\right\} \tag{16}$$

should be made with taking into consideration that

$$\left.\begin{aligned} \underline{I}_{1A} + \underline{I}'_{2A} &= \underline{I}_{mA} \\ \underline{I}_{1B} + \underline{I}'_{2B} &= \underline{I}_{mB} \end{aligned}\right\} \tag{17}$$

Then we obtain the system of equations:

$$\left.\begin{aligned} &\left(R_{1A} + jX_{1\sigma A}\right)\underline{I}_{1A} + jX_{mA}\underline{I}_{mA} - jX_C\underline{I} = 0 \\ &-\left(R'_{2A}/s_A - jX'_{2\sigma A}\right)\underline{I}'_{2A} + jX_{mA}\underline{I}_{mA} = 0 \\ &\left(R_{1B} + jX_{1\sigma B}\right)\underline{I}_{1B} + jX_{mB}\underline{I}_{mB} - jX_C\underline{I} = 0 \\ &-\left(R'_{2B}/s_B - jX'_{2\sigma B}\right)\underline{I}'_{2B} + jX_{mB}\underline{I}_{mB} = 0 \end{aligned}\right\} \tag{18}$$

The quivalent circuit presented in Fig. 2 corresponds to these equations.

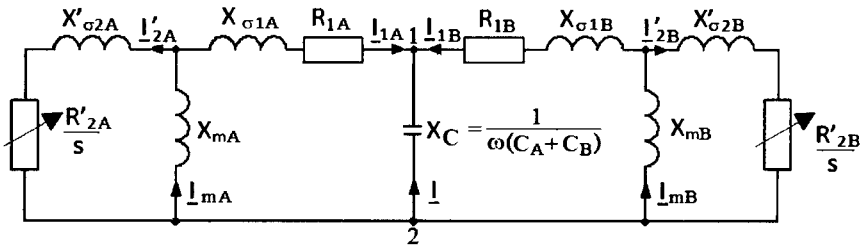

Fig. 3. The quivalent circuit of the two induction generators with capacitor excitation running in idle mode

3. PARALLEL OPERATION OF SELF-EXCITED INDUCTION GENERATORS UNDER LOAD

In general case the relation between the wattless power values of two induction generators operating in parallel under load can be determined by the equation

$$\left(Q - Q_{load}\right) = \left(Q_{1A} + Q_{1B}\right) \tag{19}$$

where:

Q – the wattless power of the capacitor battery,
Q_{load} – load wattles power,
Q_{1A}, Q_1 – the wattless magnetizing power of generators A and B.

From the formula (19) it turns out that the resultant wattless power of the external circuits, regardless of the load nature, is of capacitive character. Thus, the resultant impedance of the external circuits is of resistance-capacitive nature, as shown by

$$\underline{Z} = R - jX \tag{20}$$

Then, for the induction generators operating in parallel under load we obtain an analogous system of equations (2), namely:

$$\left.\begin{aligned}
&(R_{1A}+jX_{1A})\underline{I}_{1A}+jX_{mA}\underline{I}'_{2A}+(R-jX)\underline{I}=0\\
&js_AX_{mA}\underline{I}_{1A}-(R'_{2A}-js_AX'_{2A})\underline{I}'_{2A}=0\\
&(R_{1B}+jX_{1B})\underline{I}_{1B}+jX_{mB}\underline{I}'_{2B}+(R-jX)\underline{I}=0\\
&js_BX_{mB}\underline{I}_{1B}-(R'_{2B}-js_BX'_{2B})\underline{I}'_{2B}=0\\
&\underline{I}_{1A}+\underline{I}_{1B}-\underline{I}=0
\end{aligned}\right\} \tag{21}$$

After the same transformations as for the case of the idle mode we obtain the system of equations in the form:

$$\left.\begin{aligned}
&\underline{Z}_A\underline{I}_{1A}+\underline{Z}\underline{I}=0\\
&\underline{Z}_B\underline{I}_{1B}+\underline{Z}\underline{I}=0\\
&\underline{I}_{1A}+\underline{I}_{1B}-\underline{I}=0
\end{aligned}\right\} \tag{22}$$

where:

$$\underline{Z}_A=\left[R_{1A}-\frac{X_{mA}^2R'_{2A}s_A}{(R'_{2A})^2+(X'_{2A}s_A)^2}\right]+j\left[X_{1A}-\frac{X'_{2A}X_{mA}^2s_A^2}{(R'_{2A})^2+(X'_{2A}s_A)^2}\right]$$

$$\underline{Z}_B=\left[R_{1B}-\frac{X_{mB}^2R'_{2B}s_B}{(R'_{2B})^2+(X'_{2B}s_B)^2}\right]+j\left[X_{1B}-\frac{X'_{2B}X_{mB}^2s_B^2}{(R'_{2B})^2+(X'_{2B}s_B)^2}\right]$$

– impedances of the substitute diagrams of generators,

$\underline{Z}$ – impedance of the equivalent circuits, determined by (20).

The condition for the stable operation of induction generators running in parallel under load is, that

$$\begin{vmatrix}
\underline{Z}_A & 0 & \underline{Z}\\
0 & \underline{Z}_B & \underline{Z}\\
1 & 1 & -1
\end{vmatrix}=0 \tag{23}$$

or

$$\underline{Z}=-\frac{\underline{Z}_A\underline{Z}_B}{\underline{Z}_A+\underline{Z}_B} \tag{24}$$

i.e.

$$\underline{Z}=-\underline{Z}_{eqv} \tag{25}$$

The above speculation enable us to conclude that:

– the impedances of both the phases of the equivalent circuits and equivalent generator are equal with regard to the value, and opposite to the sign,

- the total resistance of the system is equal zero, which means that the negative resistance of the substitute generator can be considered as a generating element, the entire power of which is developed in the equivalent circuit.
- the total reactance of the system is also equal zero, which means that capacitors only are the source of the system wattless power under the load R and R-L. Their wattless power compensates the wattless powers of the generators and load powers. The values of the frequency of the voltage generated, the saturation of the magnetic circuits, and the slips of the generators become such that the total impedance of the entire system is equal zero.

The system of equations (21) after taking into consideration (16) and (17) can be finally put as:

$$\left.\begin{aligned} (R_{1A} + jX_{1A})\underline{I}_{1A} + jX_{mA}\underline{I}_{mA} + (R - jX)\underline{I} = 0 \\ -\left(\frac{R'_{2A}}{s_A} - jX'_{2A}\right)\underline{I}'_{2A} + jX_{mA}\underline{I}_{mA} = 0 \\ (R_{1B} + jX_{1B})\underline{I}_{1B} + jX_{mB}\underline{I}_{mB} + (R - jX)\underline{I} = 0 \\ -\left(\frac{R'_{2B}}{s_B} - jX'_{2B}\right)\underline{I}'_{2B} + jX_{mB}\underline{I}_{mB} = 0 \\ \underline{I}_{1A} + \underline{I}_{1B} - \underline{I} = 0 \end{aligned}\right\} \qquad (26)$$

The equivalent circuit presented in Fig. 3, where between the points 1 and 2 the impedance $\underline{Z}$=R-jX has been connected corresponds to the above system of equations. The obtained system of equations (26), after solving it, can be used for the analysis of the operation of the induction generators running in parallel under load.

4. PARALLEL OPERATION OF THE SELF-EXCITED INDUCTION GENERATORS WITH THE DIFFERENT ROTATIONAL SPEED OF THEIR SHAFTS

The different rotational speed of the shafts of the induction generators running in parallel results in irregular load distribution over individual generators. The consequence of this is the decrease in the use of the power of generators. One of the basic issues of the analysis of parallel operation of generators is to determine the conditions for the maximum use of the power of the system of two generators in various operational circumstances. This issue constitutes the subject of the next part of this paper.

The analysis of the operation of two induction generators running with different rotational speed of their shafts will be carried out with the following assumptions:

- two generators of identical parameters, power, and exciting capacitor battery capacitance are considered,
- the angular velocity of the A generator shaft is higher than that of the B generator shaft, i.e.

$$\omega_{wA} > \omega_{wB}$$

where ω_A = const, and ω_B = const, too.

The induction machine of the shaft lower angular velocity, depending on the generator system load level, can run in various operation modes: as generator, idle, and as motor. If initially this machine was running in the generator mode and the load level was decreased so that $\omega = \omega_w$ (ω - field angular velocity), then this generator goes to idle mode. With further decrease of the load the generator goes to the motor operation mode and it should be disconnected from the common busbars.

In further speculations it is assumed that both generators operate in parallel for the grid in the entire range of load, i.e. from zero to the maximum possible.

Idle mode

In this mode the field angular velocity ω is expressed with the relationship:

$$\omega = \frac{1}{p\sqrt{LC}} \tag{27}$$

or

$$\omega = \frac{\omega_{wA} + \omega_{wB}}{2} \tag{28}$$

The later formula shows, that with the assumption $\omega_{wA} > \omega_{wB}$, $\omega > \omega_{wB}$. Therefore the B machine operates with additional slip and remains in the motor mode. With $|\underline{Z}| = \infty$ the generator system is in idle mode, but individual generators run with the same slip with regard to the value, and opposite to the sign, and are loaded symmetrically. The absolute slip value is proportional to the difference $\Delta\omega_{wA} = \omega_{wA} - \omega_{wB}$.

Summarizing, it can be stated that in the idle mode, when $\omega_{wA} = \omega_{wB}$, the active power generated by one of the generators is consumed by the other. The corresponding to this power electromagnetic moment is acting in the direction opposite to the turning moment of the A generator and accordingly to the direction of the B generator spin. Thus this moment can be named the synchronizing moment.

Symmetrical load state

The relations between the angular velocities of fields and shafts of generators are determined by the relationships applied for all operation modes, namely:

$$\left.\begin{aligned} \omega &= \frac{\omega_{wA}}{(1 - s_A)} \\ \omega &= \frac{\omega_{wB}}{(1 - s_B)} \end{aligned}\right\} \tag{29}$$

With the assumption made earlier that $\omega_{wA} > \omega_{wB}$, the A generator slip remains negative, which means that this generator is always in the generator mode. For working loads it can be put, that:

$$\frac{s_B}{s_A} = \frac{P_B}{P_A} \tag{30}$$

i.e. the slip ratio is then proportional to the ratio of powers developed by the individual generators.

Neglecting the losses it can be stated that

$$P_A + P_B = P \tag{31}$$

where P is the power released in the load.

From (30) and (31) it results that

$$s_B = s_A\left(\frac{P}{P_A} - 1\right) \tag{32}$$

As it has already been mentioned above, the slip of the second generator can reach various levels, depending on the load value. And so with $P < P_A$ the active power balance can be expressed as

$$P_A = P_B + P \tag{33}$$

which means that the B generator is consuming the active power ($s_B > 0$). With $P_A = P$ the B generator operates in idle mode ($s_B = 0$). With $P > P_A$ the slip s_B becomes negative (see formula (32)). Both generators produce active power to the load, and the power generated by them can be determined by (31). However, the loads of both generators are not the same. Since $P_A > P_B$, the power of the B generator is not fully used, and the $|s_B|$ value is smaller then the rated one.

The limit slip value for the B generator corresponds to the rated slip of the A generator. This value can be determined from the formula (32), which in this case can be expressed as

$$s_{Bg} = s_{AN}\left(\frac{P_g}{P_{AN}} - 1\right) \tag{34}$$

where P_g is the limit value of the power of the generator system at the rated load of the A generator and it is equal

$$P_g = P_{AN} + P_{Bg} \tag{35}$$

In the expression (35) P_{Bg} is the limit value of the B generator power corresponding to the negative s_{Bg} limit slip.

The considerations presented above show that the closer the s_{Bg} value is to the s_{BN} rated value the higher is the index of the use of the energy system.

In order to determine the factors affecting the s_{Bg} value we introduce the concept of the generator power use coefficient

$$K = \frac{P}{2P_{AN}} \tag{36}$$

which for s_{AN} , s_{Bg} slips it will be designated as K_N .
Therefore

$$K_N = \frac{P_g}{2P_{AN}} \tag{37}$$

which with taking into consideration (35), where

$$P_{Bg} = \frac{s_{Bg}}{s_{AN}} P_{AN}$$

gives us

$$K_N = \frac{s_{AN} + s_{Bg}}{2s_{AN}} \tag{38}$$

This means that for $|s_A| > |s_{AN}|$ and $|s_B < s_{Bg}|$ slips the use of the power of generators decreases along with the decrease of the use coefficient

$$K = \frac{s_A + s_B}{2s_A} \tag{39}$$

In order to define the relationship between the slip of the generators and the angular velocities of their shafts we introduce the coefficient

$$k = \frac{\omega_{wA}}{\omega_{wB}} \tag{40}$$

and use the relationships (29).
By equating the right hand sides of these formulas we obtain

$$s_B = 1 - \frac{1 - s_A}{k} \tag{41}$$

This relationship above shows that the best use of the generator power is achieved at the rated s_{AN} slip of the A generator and the corresponding negative s_{Bg} slip of the B generator. Then

$$s_{Bg} = 1 - \frac{1 - s_{AN}}{k} \tag{42}$$

As it can be seen the s_{Bg} slip is the function of two independent variables s_{AN} and k, and in general case it can assume positive or/and negative values, as well as it can be equal zero. For the concrete generator s_{AN} = const, whereas s_{Bg} = f(k).
(42) also shows that the s_{Bg} assumes negative values when

$$(1 - s_{AN}) > k \tag{43a}$$

or

$$|s_{AN}| > k - 1 \tag{43b}$$

where

$$k - 1 = \frac{\omega_{wA} - \omega_{wB}}{\omega_{wB}} \tag{44}$$

is equal to the relative value of the difference of angular velocities of generator shafts, whereas the reference value is ω_{wB}. This value can be considered as the slip of the B generator shaft with regard to the A generator rotor, and expressed as a fraction of the ω_{wB} velocity.

Conclusion:
The s_{Bg} slip is negative if the absolute value of the rated s_N slip of generators is bigger then the relative difference of the angular velocity of the generator shafts.

The use of the second generator (B) at operation in parallel makes sense within the range of negative slips only. However, with sudden changing of load, when load peaks exceed the maximum allowable short-term overload of the first generator (A), the simultaneous operation of both generators to supply the load becomes just reasonable.

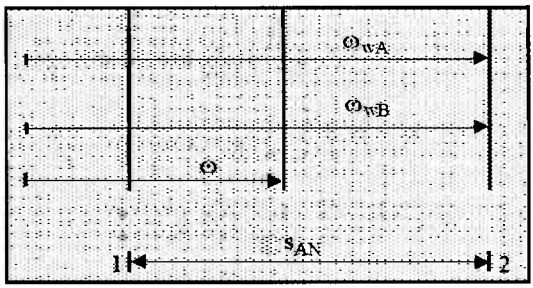

Fig. 4. Operation modes for conditions: $\omega_{wA} = \text{const}$, $\omega_{wB} = \text{const}$, $\omega_{wA} \geq \omega_{wB}$, $s_A = s_{AN}$, $s_{Bg} = s_{AN}$

Below all possible operation modes of generators running in parallel are examined, with the existing difference of the angular velocity of shafts and changing load.

It was mentioned earlier that the operation mode of the generator with the lower angular velocity of its shaft depends on load level and the $(k-1)/|s_N|$ ratio. The possible operation modes for the second (B) generator with $s_{AN} = \text{const.}$ can be different. In Fig. 4a case is shown when shaft angular velocities and slips of generators are equal, i.e. $s_{Bg} = s_{AN}$. In these circumstances, with any load level, the slip of the B generator is always negative ($s_B < 0$). Because, as it results from (42)

$$k - 1 = s_{Bg}k - s_{AN} \tag{45}$$

then with $k > 1$ and the operation of the A generator in the rated mode, the B generator runs in idle mode if

$$k - 1 = |s_{AN}| \tag{46}$$

whereas $\omega_{wB} = \omega$ (see Fig. 5).

With decreasing the load the frequency of the generated voltage rises and the B generator goes to the operation mode with positive slip ($\omega > \omega_{wB}$, $s_B > 0$). The range of negative generator A slips, for which the generator under discussed conditions of operation works in generator mode, presents on Fig. 4 section $\overline{12}$. Similarly sections on Figures 5÷7 represent the same for another discussed conditions of operating.

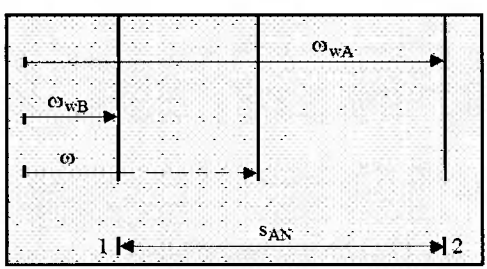

Fig. 5. Operation mode of generators for conditions: $\omega_{wA} = \text{const}$, $\omega_{wB} = \text{const}$, $\omega_{wA} \geq \omega_{wB}$, $s_A = s_{ANg}$, $s_{Bg} = 0$

In idle mode the frequency reaches the maximum value determined by the average angular velocity of generators (dotted line in Fig. 5). If now the load is increased, then with $P = P_{AN}$ we come again to the state $\omega_{wB} = \omega$, $s_{Bg} = 0$. Further increase of the load leads to the situation when $\omega_{wB} > \omega$ and the operation of the B generator with negative slip, but the slip value of the A generator exceeds the rated s_{AN} value of the slip.
The operation of both generators in parallel for the load is possible only when the (43b) condition is met, what is illustrated in Fig. 6.

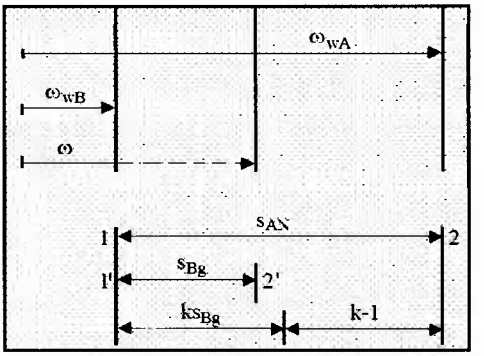

Fig. 6. The operation modes for the conditions: $\omega_{wA} = \text{const}$, $\omega_{wB} = \text{const}$, $\omega_{wA} \geq \omega_{wB}$, $s_A = s_{AN}$, $s_{Bg} < 0$

Since $\omega_{wB} > \omega$, then the s_{Bg} slip is < 0, and from (45) we have that:

$$k - 1 = |s_{AN}| - |s_{Bg}|k \tag{47}$$

The expression (47) determines the relationship between the rated slip of the A generator and the relative difference of the angular velocities of the shafts of both generators at the maximum possible (limit) power of the system of both generators, corresponding to the negative s_{Bg} slip of the B generator. The range of the s_B negative slips of the B generator corresponds with the section $\overline{1'2'}$ in Fig. 6.

In Fig. 7 it is shown that the change of the slip of the A generator from 0 to s_{AN} forces the B generator to run, and this generator, when running, consumes power from the common grid. In this state the

$$k - 1 = |s_{AN}| + |s_{Bg}|k \tag{48}$$

condition is met, which results in the fact that if

$$\frac{k-1}{s_{AN}} > 1 \tag{49}$$

then the simultaneous operation of the generators for the common load is impossible.

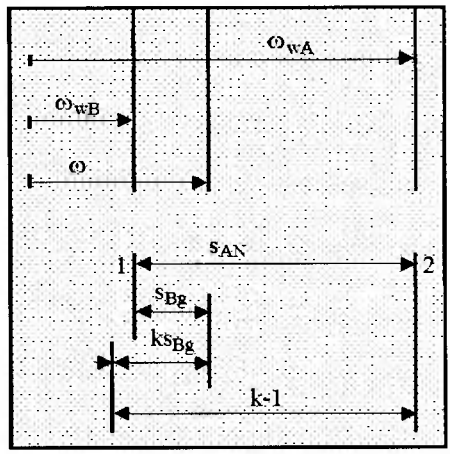

Fig. 7. Operation in parallel for the conditions: $\omega_{wA} = \text{const}$, $\omega_{wB} = \text{const}$, $\omega_{wA} \geq \omega_{wB}$, $s_A = s_{AN}$, $s_{Bg} < 0$

The energy characteristic of the system of two generators operating in parallel can be defined in some different ways [4, 5, 6], but the comparison of them is always based on the comparison of the power use indices. By transforming (38) and (39) with taking into consideration (41) and (42) we have:

$$K_N = \frac{1}{2k}\left(k + 1 + \frac{k-1}{s_{AN}}\right) \tag{50}$$

$$K = \frac{1}{2k}\left(k + 1 + \frac{k-1}{s_A}\right) \tag{51}$$

where s_A is the slip corresponding to any P_1 power lower than the rated one. From the formulas (50) and (51) it results that with the generators running in parallel the inequality $K_N > K$ is always fulfilled, since $|s_{AN}| > |s_A|$.

Conclusion:

The use of the power of induction generators running in parallel depends on the load level and angular velocity of their shafts.

On the basis of the considerations carried out it is possible do determine the value of the coefficients which characterise the maximum possible use of generators depending on operation conditions. This is presented in graphical form in Fig. 8. The conditions of the operation of generators is described by the characteristic family

$$k - 1 = f\left(\frac{s_{Bg}}{s_{AN}}\right) \tag{52}$$

at $s_{AN} = \text{const}$.

The algorithm used at the creation of the Fig. 8 is as follows:
- for the assumed s_{AN} slip value = const. various k ratio values are presumed,
- from (42) the values corresponding to them are found; it is convenient to express the s_{Bg} slip in relative units with reference to s_{AN}.
- The s_{Bg}/s_{AN} ratio is > 0 if $s_{Bg} < 0$, which demonstrates that to the operation of both generators in the generator mode the first quarter of Cartesian coordinate system corresponds. The s_{Bg}/s_{AN} ratio is < 0 if $s_{Bg} > 0$, to which the second quarter of coordinate system corresponds;
- after the calculation of the k-1 values corresponding to the k ratios we obtain the data necessary to draw the $k - 1 = f(s_{Bg}/s_{AN})$ straight line at s_{AN} = const.
- the characteristic for other slip values is calculated in the same way.

In Fig. 8 the relationship $K_N = f(s_{Bg}/s_{AN})$ at s_{AN} = const. is presented to. This relationship is based on (50) for various k values. If this relationship is to be expressed in relative units then, with the use of this drawing, the limit energy indices can be determined for the two induction generators operating in parallel for various (s_{Bg}/s_{AN}) ratio values, s_{AN} slips, and relative k-1 differences in rotational speeds of the shafts of both generators.

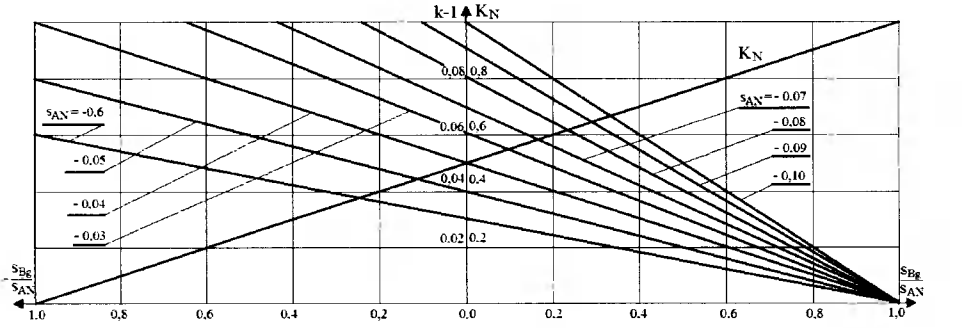

Fig. 8. The relationship between the coefficients of the use of the power of the induction generators operating in parallel and the load conditions

Example:

For the difference in shaft rotational speeds of both generators amounting to 3 percent and the A generator operating with the s_{AN} rated slip = –0.05 the s_{Bg}/s_{AN} ratio = 0.4, and the K_N coefficient of power use = 0.7.

The relationships mentioned above show, that in fact:

$$s_{Bg} = 0.4 s_{AN} = -0.02$$

$$P_{Bg} = \frac{0.02}{0.05} P_{AN} = 0.4 P_{AN}$$

$$K_N = \frac{P_{AN} + 0.4 P_{AN}}{2 P_{AN}} = 0.7$$

Therefore, the second quarter of the coordinate system characterizes the operation of the induction generators in the mode when one of them is loaded with the rated load and supplies its power to the common grid, whereas $\omega_{wA} > \omega > \omega_{wB}$, and the second generator consumes energy from the grid ($s_B > 0$).

With the

$$k = \frac{1 - s_{AN}}{1 + s_{AN}} \tag{53}$$

condition met the power supplied to the load amounts to zero.

Conclusion:
With s_{AN} = const *the use of the power of the induction generators operating in parallel is the higher the lower is the difference in the rotational speed of their shafts. The highest indices of the use of the power generated by generators are achieved when* s_B / s_A *ratios are positive, i.e. when both machines operate in the generator mode.*

With the assumption that k = const the more effective use of the generators operating in parallel can be achieved when machines of increased slip are used. As the s_{AN} slip increases also the s_{Bg}/s_{AN} ratio increases, and in this ratio the increments of the numerator and denominator are the same. In this case, the improvement on the use of the power of generators is achieved by increasing the $|s_{Bg}|$ slip of the B generator with the A generator loaded with the rated load (Fig. 9).

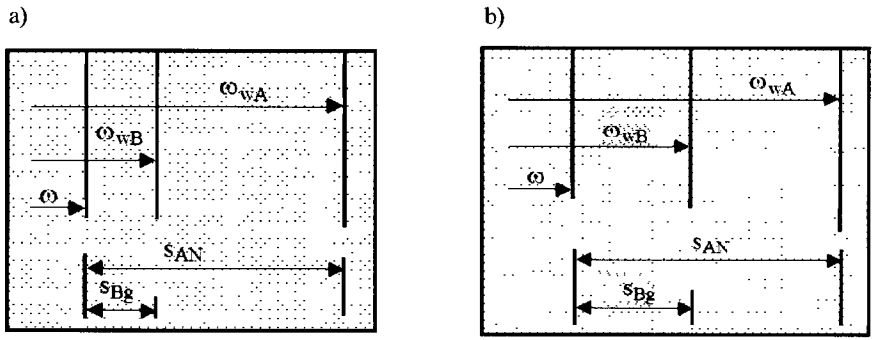

Fig. 9. The impact of the rated slip on the use of the power of the induction generators operating in parallel with different rotational speed of their shafts for slip ratios: a) $s_{Bg}/s_{AN} \approx 0.2$, b) $s_{Bg}/s_{AN} \approx 0.3$

When evaluating the energy indices of the induction generators running in parallel the following relationship can be useful:

$$\left(\frac{s_{Bg}}{s_{AN}}\right) = f(s_{AN}) \text{ at } k = \text{const}$$

which is analogous to that presented in Fig. 10.

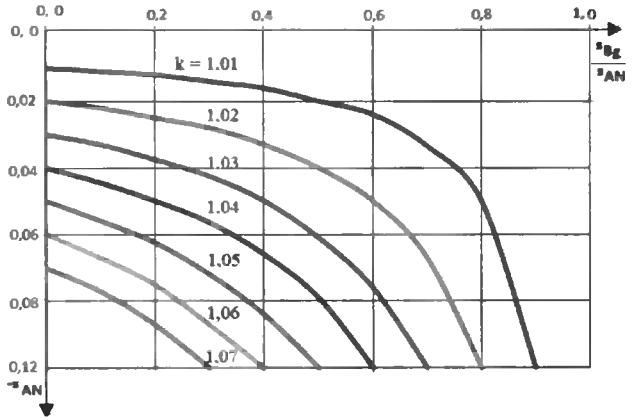

Fig. 10. $K_{Nf} = f(s_{Bg}/s_{AN})$ relationship at $s_{AN} = const$

Example:
The Fig 7 and 9 show, that for k = 1.02 at $s_{AN} = -0.05$ the coefficient of the use of the power of machines K = 0.8. The B generator power is calculated from

$$P_{Bg} = \frac{s_{Bg}}{s_{AN}} P_{AN} = 0{,}6P_{AN} \tag{54}$$

If the A generator with the rated s_{AN} slip = –0.1 is applied, then the K_N coefficient of the use of the power of machines = 0.9. Thus, increasing the rated slip of the A generator twice makes the use of the power of the machines increased by circa 10 percent.

The increase of the use the power of the induction generators running in parallel with a given slip is also possible by decreasing the difference of the rotational speed of the shafts of the machines. Decreasing it, e.g. so that at $s_{AN} = -0.05$ the k coefficient drops from k = 1.02 to k = 1.01 also makes the coefficient of the use of the power of machines higher and reaching K = 0.9.
The presented here considerations on the use of the power of machines operating in parallel concerned the most reasonable case when $P_A = P_{AN}$. In the case when $P_A < P_{AN}$, then the coefficient of the use of the power of machines should be determined according to (36) and (51).

CONCLUSIONS

1. Because induction generators with capacitance excitation can run parallel with different rotating speed of shafts, is necessary to define conditions of work ensuring operation of both generators in the range of negative operation slips, keeping as possible, big coefficient of productivity machine power.
2. With different rotational speed of the shafts of generators the load spreads on individual generators unevenly, even when both generators are identical. The generator with higher rotational speed of its shaft supplies higher active power, and consumes higher wattless power. The regulation function of the system is played here by driving motors.
3. The use of the power of the generators running in parallel depends on the difference in the rotational speed of shafts and rated slips. Decreasing the Δn_w difference in the

rotational speed of shafts or increasing the rated slip with unchanged Δn_w value makes the coefficient of the use of the power of machines higher.

4. The best use of the power of the machines running in parallel with different rotational speed of their shafts can be achieved when one of the generators runs with the rated slip, and the second one – with negative limit slip corresponding to the first one. The limit slip of the second slip is negative when the absolute value of the rated slip of the first generator is higher than the relative difference of the rotational speed of both shafts.

BIBLIOGRAPHY

[1] Al-Bahrani A.H., Malik N.H., 1993. Stady state analysis of parallel operated self--excited induction generators. IEE Proc., No. 140.
[2] Farred F.A., Palle B., Simoes M.G., 2005. Full expandable mode of parallel self--excited induction generators. IEE Proc. Electr. Power Appl., Vol. 152, No. 1.
[3] Shibata F., Itoi T., 1960. Analysis of "SK" Generator (self-excited A.C. generator for ship using new methods of parallel running) and its application. Journal Detail, No. 100.
[4] Sung-Chun K., Li W., 2004. Analysis of parallel-operated self-excited induction generators Feeding an induction motor with a long-shunt connection.Electric Power Components and Systems, Vol. 32.
[5] Wang L., Lee C.H., 1998. A novel analysis of parallel operated self-excited inductions generators. IEEE Trans. Energy Convers, No. 13.
[6] Zubkov J.D., 1960. Parallelnaja rabota asinchronnych generatorov c kondensatornym vozbużdeniem. Trudy Kazachsk. SChI, t. 8, vyp. 3.

ANALIZA PRACY RÓWNOLEGŁEJ PRĄDNIC INDUKCYJNYCH O WZBUDZENIU KONDENSATOROWYM

Streszczenie

W artykule rozpatrzono pracę równoległą prądnic indukcyjnych o wzbudzeniu kondensatorowym. Omówiono krótko najprostsze sposoby włączenia prądnic do pracy równoległej. Przedstawiono model matematyczny prądnic pracujących równolegle dla stanów statycznych. Określono warunki najlepszego wykorzystania mocy prądnic pracujących równolegle.

Słowa kluczowe: prądnica indukcyjna, praca równoległa, stany statyczne

UNIWERSYTET TECHNOLOGICZNO-PRZYRODNICZY
IM. JANA I JĘDRZEJA ŚNIADECKICH W BYDGOSZCZY
ZESZYTY NAUKOWE NR 257
ELEKTROTECHNIKA 15 (2010) 43-51

APPLICATION OF THE COMBINATORIAL SEQUENCING THEORY FOR INNOVATIVE CODED DESIGN OF SIGNALS

Włodzimierz Riznyk, Grzegorz Meckien

Instytut Elektrotechniki, Wydział Telekomunikacji i Elektrotechniki
Al. Prof. S. Kaliskiego 7, 85-789 Bydgoszcz

Summary: The paper deals with coded design of signals of remarkable correlation quality or minimizing of codes with respect to correlation function owing to the best spatially distributed impulses of coded signals. The method based on application of remarkable properties of particular combinatorial structures called "Gold Numerical Rings" (GNR)s, provided to simplify finding the optimal variants for synthesis of the signals is described. Method for coded design of the signals using GNRs, can be well applied in electronic engineering, control systems, telecommunications and radio-engineering.

Keywords: signal, code, autocorrelation function, optimisation.

1. INTRODUCTION

Development of the Combinatorial Sequencing theory is known to be of very important for coded design and signal processing of fine resolution in spatially or temporally distributed systems. It is a great class of the appropriate mathematical problems based on development of the technologically optimum distributed systems theory. These problems involve applications of the theory to control and coded design of signals for electrical engineering and power electronics, communications and optical electronics, as well as the other areas to which the theory can be applied.

2. COMBINATORIAL NUMERICAL SEQUENCES

A lot of well-known engineering technologies or systems with non-uniform structure are very distant from perfect fulfilment of the design with respect to performance reliability, resolving ability and the other significant operating characteristics of the system.

Below you can find some structural diagrams of the two mathematical models of systems, namely rulers contained four ($n = 4$) each marks; the first ruler contains uniform arranged marks (Fig.1, a) while the second one has a non-uniform arrangement of marks (Fig.1, b).

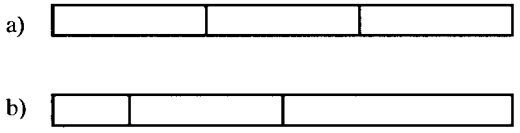

Fig. 1. Structural diagrams of rulers with uniform (a) and non-uniform (b) arrangement of marks

The ruler with uniform arrangement of marks (Fig.1, a) make it possible to reproduce only 3 precision linear distances $L/3$, $2L/3$ and L, where L - length of the all ruler, while ruler with non-uniform structure (Fig.1, b) provides an ability to reproduce much more number of distances than previous ruler due to the more number of distinct distances between marks. Comparing the structural diagrams (Fig.1, a) and (Fig.1, b) from information possibility point of view, we see that rulers with non-uniform arrangement of marks provide an ability to reproduce the more useful information, because a redundant information is equally its loss. In order to improve the resolving ability of the ruler with non-uniform structure it is necessary to arrange marks so that maximum number of precision results of reproduced distances with fixed step can be obtained without increasing of the mark number. In this connection it is the question on finding general solution of the problem [1-3]. Development of idea in this direction has been achieved by S. W. Golomb, who suggests the new design for constructing these rulers with non-uniform positioning of marks, where each pair of marks is positioned at various distances, and the set of all distances corresponds to the natural numbers, besides in the best case the set exhausts of the natural numerical row [1]. An example of Golomb "Ideal" ruler of length six ($L = 6$) units with marks 0, 1, 4, 6 is given below (Fig.2).

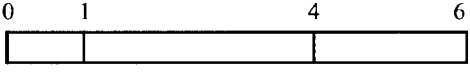

Fig. 2. The Golomb "Ideal" ruler of length six ($L = 6$) units

The remarkable property of the Ideal ruler in comparison with usual ruler is non-uniform positioning of marks (0, 1, 4, 6) so, that the each next in turn pair of the marks is within the distance from 0 to $L = 6$ as follows:

$$1 = 1 - 0 \qquad 2 = 6 - 4 \qquad 3 = 4 \quad 1$$
$$4 = 4 - 0 \qquad 5 = 6 \quad 1 \qquad 6 = 6 - 0$$

Note, that created set of distance values corresponds to the natural numerical row 1, 2,..., 6.

The Golomb Ideal ruler (Fig.2) 0, 1, 4, 6 containing three intersections {1, 3, 2}, where $1 = 1 - 0$, $3 = 4 - 1$, and $2 = 6 - 4$, allows an enumeration of all numbers $1 = 1$, $2 = 2$, $3 = 3$, $4 = 1 + 3$, $5 = 3 + 2$, $6 = 1 + 3 + 2$ exactly once ($R = 1$).

Here is a graphic model of Ideal numerical sequence {1, 3, 2} of daisy-chain topology (Golomb Ruler) for six ($L = 6$) units, namely the Ideal numerical sequence with parameters $n = 3$ and $R = 1$ (Fig. 3).

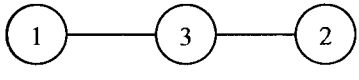

Fig. 3. A graphic model of the Ideal numerical sequence {1, 3, 2} of daisy-chain topology with parameters $n = 3$ and $R = 1$

Unfortunately, there are not existing Ideal Numerical Sequences with more than three ($n > 3$) intersections. The problem is known to be of great importance for development of regular method based on the idea of "ideal sequences" for finding optimal placement of more than three structural elements in system [2, 3].

It is easy to calculate, that in comparison to usual ruler with the same number of marks ($n = 4$), the Ideal ruler is exactly a double number of reproduced distance values (from 3 to 6) at the identical measuring range, and accordingly provides improving of resolving ability of devices and systems, based on the underlying design technique. So, the development of new direction in fundamental and applied research into informatics and systems engineering, using innovative methodologies based on the Combinatorial Sequencing Theory to be of very important for improving such quality indices as resolving ability, precision, speed, performance reliability, functionality and other significant characteristics of the system.

2.1. SUMS ON CHAIN ORDERED NUMERICAL SEQUENCE

Let us consider the numerical n-stage chain sequence of distinct positive integers $\{k_1, k_2,\dots, k_n\}$, where we require all terms in each sum to be consecutive elements of the sequence:

$$
\begin{array}{lll}
k_1, & k_2,\dots & k_n \\
k_1 + k_2, & k_2 + k_3,\dots & k_{n-1} + k_n \\
k_1 + k_2 + k_3, & k_2 + k_3 + k_4,\dots & k_{n-2} + k_{n-1} + k_n \\
\dots\dots & \dots\dots & \dots\dots \\
k_1 + k_2 + \dots + k_n & &
\end{array}
$$

We can calculate all S_n sums of the terms in the numerical n-stage chain sequence of distinct positive integers $K_n = \{k_1, k_2,\dots, k_i,\dots k_n\}$, where we require all terms in each sum to be consecutive elements of the sequence. Clearly such a maximum sum is the sum S_{max} of all n elements:

$$S_{max} = k_1 + k_2 + \dots + k_i + \dots + k_n . \tag{1}$$

A sum of consecutive terms in the chain sequence can have any of the n terms as its starting point p_j, and finishing point q_j , and can be of any length (number of terms) from 1 to n. So, the each j-th numerical pair (p_j, q_j), p_j, $q_j \in \{1, 2,\dots, n\}$ corresponds to sum $S_j = S\,(p_j, q_j)$, is equal as here:

$$S_j = S\,(p_j,q_j) = \sum_{i=p_j}^{q_j} k_i\ ,\ p_j \le q_j. \tag{2}$$

An ordered numerical pair (p_j,q_j) determines the sum $S\,(p_j,q_j)$ in the numerical n-stage chain sequence, and it is a numerical code of the sum. The all sums of consecutive terms, calculated by (2), can be illustrated graphically by the Table 1. To see this, we observe the maximum number of distinct sums is

$$S'_{max} = 1 + 2 + \dots + n = n\,(n + 1)/2. \tag{3}$$

The ideal ordered-chain sequence is such numerical n-stage of distinct positive integers $k_1, k_2, \dots , k_n$, which exhausts the natural row of numbers written down into cells of the table 1. Table of sums of consecutive terms in ordered-chain sequence could be

used for research of numerical sequences in order to speed up finding ideal or optimal solutions.

Table 1. Sums of consecutive terms in ordered -chain sequence

p_j	q_j				
	1	2	...	n 1	n
1	k_1	$\sum_{i=1}^{2} k_i$	...	$\sum_{i=1}^{n-1} k_i$	$\sum_{i=1}^{n} k_i$
2		k_2	...	$\sum_{i=2}^{n-1} k_i$	$\sum_{i=2}^{n} k_i$
...			...		...
$n-1$				k_{n-1}	$\sum_{i=n-1}^{n} k_i$
n					k_n

Easy to see (Table 1) the maximum number C of such sums is equal to the sum $k_1 + k_2 + \ldots + k_n = C$ of all integers:

$$C = 1 + 2 + \ldots + n = (n^2 - n)/2 \tag{4}$$

For example, if we deals with research of numerical 3-stage of distinct positive integers $\{1, 3, 2\}$, where $k_1 = 1$, $k_2 = 3$, $k_3 = 2$, than table 1 assumes the next shape (Table 2).

We observe, Table 2 contains the set of all $S'_{max} = n(n + 1)/2 = 6$ sums to be consecutive elements of the 3-stage chain sequence $\{1, 3, 2\}$, and each sum from 1 to 6 occurs exactly once. So, the 3-stage chain sequence $\{1, 3, 2\}$ is the Ideal ruler.

Table 2. Sums of consecutive terms in chain sequence $\{1, 3, 2\}$.

p_j	q_j		
	1	2	3
1	$k_1 = 1$	$\sum_{i=1}^{2} k_i = 4$	$\sum_{i=1}^{3} k_i = 1 + 3 + 2 = 6$
2		$k_2 = 3$	$\sum_{i=2}^{3} k_i = 3 + 2 = 5$
3			$k_3 = 2$

2.2. SUMS ON ORDERED-RING NUMBERS

If we regard the chain sequence K_n as being cyclic, so that element k_n is followed by k_1, we call this a ring sequence. A sum of consecutive terms in the ring sequence can have any of the n terms as its starting point p_j, and finishing point q_j, and can be of any length (number of terms) from 1 to $n - 1$. In addition, there is the sum S_n of all n terms, which is the same independently of the starting point.

Table of sums of consecutive terms in ordered-ring sequence $Kn = \{k_1, k_2, \ldots, k_i, \ldots k_n\}$ is demonstrated below (Tabl.3).

Table 3. Sums of consecutive terms in ordered -ring sequence

p_j	q_j				
	1	2	...	$n-1$	n
1	k_1	$\sum_{i=1}^{2} k_i$	...	$\sum_{i=1}^{n-1} k_i$	$\sum_{i=1}^{n} k_i$
2	$\sum_{i=1}^{n} k_i$	k_2	...	$\sum_{i=2}^{n-1} k_i$	$\sum_{i=2}^{n} k_i$
...			...		...
$n-1$	$\sum_{i=n-1}^{n} k_i + k_1$	$\sum_{i=n-1}^{n} k_i + \sum_{i=1}^{2} k_i$	...	k_{n-1}	$\sum_{i=n-1}^{n} k_i$
n	$k_n + k_1$	$k_n + \sum_{i=1}^{2} k_i$	...	$\sum_{i=1}^{n} k_i$	k_n

A sum of consecutive terms in the ring sequence can have any of the n terms as its starting point p_j, and finishing point q_j, and can be of any length (number of terms) from 1 to n - 1. So, each j-th numerical pair (p_j, q_j), $p_j, q_j \in \{1, 2, \ldots, n\}$, corresponds to sum $S_j = S(p_j, q_j)$, and can be calculated in case, when $p_j \leq q_j$, by equation:

$$S_j = S(p_j, q_j) = \sum_{i=p_j}^{q_j} k_i \,. \tag{5}$$

In case $p_j > q_j$ a ring sum can be calculated by

$$S_j = S(p_j, q_j) = \sum_{i=1}^{q_j} k_i + \sum_{i=p_j}^{n} k_i \,. \tag{6}$$

Easy to see from the table 3, that the maximum number of distinct sums S_n of consecutive terms of the ring sequence is

$$S_n = n(n - 1) + 1 \tag{7}$$

Comparing the equation (4) and (7), we see that the number of sums S_n for consecutive terms in the ring topology is nearly double the number of sums S'_{max} in the daisy-chain topology, for the same sequence K_n of n terms.

3. GOLD NUMERICAL RINGS

An n-stage ring sequence $K_n = \{k_1, k_2, \ldots, k_i, \ldots k_n\}$ of natural numbers for which the set of all S_n circular sums consists of the numbers from 1 to $S_n = n(n - 1) + 1$, that is each number occurring exactly once, is called an "Gold Numerical Ring" (GNR) [4].

Here is an example of a numerical ring sequence with $n = 4$ and $S_n = n(n-1) + 1 = 13$, namely $\{1, 2, 3, 7\}$, where $k_1 = 1$, $k_2 = 2$, $k_3 = 3$, $k_4 = 7$.

Table of circular sums for the sequence is given below (Table 4).

Table 4. Table of circular sums for numerical ring sequence $\{1, 2, 3, 7\}$

p_j	q_j			
	1	2	3	4
1	1	3	6	13
2	13	2	5	12
3	11	13	3	10
4	8	10	13	7

Table 4 is calculated in similar way than above, using equations (4) and (5). To see this table 4 contains the set of all $S_n = n(n-1) + 1 = 13$ sums to be consecutive elements of the 4-stage ring sequence $\{1, 2, 3, 7\}$, and two sums (3 and 10) occur twice, while two are absent (4 and 9). We say, this numerical ring sequence is not ideal construction.

Next, here is an example of a numerical ring sequence with $n = 4$ and $S_n = n(n-1) + 1 = 13$, where $k_1 = 1$, $k_2 = 3$, $k_3 = 2$, $k_4 = 7$.

Table of circular sums for the sequence is given below (Table 5).

Table 5. Circular sums for numerical ring sequence $\{1, 3, 2, 7\}$

p_j	q_j			
	1	2	3	4
1	1	4	6	13
2	13	3	5	12
3	10	13	2	9
4	8	11	13	7

Table 5 is calculated in similar way than above, using equations (4) and (5). To see this table 2 contains the set of all $S_n = n(n-1) + 1 = 13$ sums to be consecutive elements of the 4-stage ring sequence $\{1, 3, 2, 7\}$, and each sum from 1 to $n - 1$ occurs exactly once. So, the ring sequence $\{1, 3, 2, 7\}$ is an Gold Numerical Ring (GNR) with n = 4.

Here is a graphical representation of the Gold Numerical Ring containing four ($n = 4$) elements $\{1, 3, 2, 7\}$.

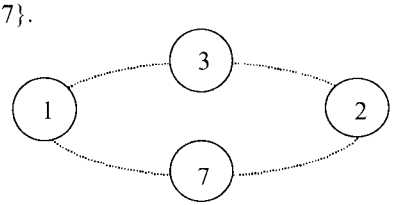

Fig. 4. A graph of Gold Numerical Ring containing four ($n = 4$) elements $\{1, 3, 2, 7\}$.

The Gold Numerical Rings (GNR)s are cyclic sequences of integers which form perfect partitions of a finite interval $[1, s]$ of integers. Sums of connected sub-sequences of any GNR enumerate the set of integers $[1, s]$ exactly λ-times. For example, circular sums of cyclic sequence $\{1, 3, 2, 1\}$ enumerate the next set of integers $[1, s = 6]$:

1 = 1	and	1 = 1,
2 = 2	and	2 = 1 + 1,
3 = 3	and	3 = 2 + 1,
4 = 1 + 3	and	4 = 1 + 2 + 1,
5 = 3 + 2	and	5 = 1 + 1 + 3,
6 = 1 + 3 + 2	and	6 = 3 + 2 + 1.

Here we see that cyclic sequence {1, 3, 2, 1} enumerate the set of integers [1, s = 6] exactly twice (λ = 2). Hence, this sequence is GNR with parameters n = 4, λ = 2 (Fig.5).

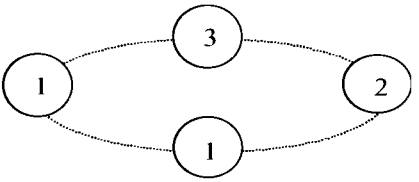

Fig. 5. A graph of Gold Numerical Ring containing four (n = 4) elements {1, 3, 2, 1}.

Theoretically, there are exist an endless number of GNRs .

So, the development of the new direction in fundamental and applied research into electronic engineering, using innovative methodologies based on the Combinatorial Sequencing theory to be of very important for improving such quality indices as resolving ability, performance reliability, and other significant characteristics of the system.

4. APPLICATION OF THE GNRs FOR CODED DESIGN OF SIGNALS

Let us regard a code sequence μ with N positions, where $\mu = \{\mu_i : i = 0, 1, \ldots N-1\}$. Periodical autocorrelation function of the code sequence is given [1] by

$$R_\mu(m) = \sum_{i=0}^{N-1} \mu_i \mu_{i+m} \tag{8}$$

where:

m = τ/τ_0 – a certain number, ($\tau > \tau_0$),
τ – a phase shift.

As long as products (+1) · (+1) and (–1) · (–1) give numbers (+1), while (+1) · (–1) and (–1) · (+1) – numbers (–1), we can write down:

$$R_\mu(m) = R = N - 4(k - \lambda) \tag{9a}$$

$$\lambda(N-1) = k(k-1) \tag{9b}$$

In order to design N-stage code sequence of fine autocorrelation function using GNR $\{k_1, k_2, \ldots k_i, \ldots k_n\}$ enough to write n symbols "+1" of the code into positions, calculated by equation:

$$x_l = \sum_{i=1}^{l} k_i \qquad l = 1,2,\ldots,n, \tag{10}$$

while the other $S - n$ position - symbols "–1".

Let us configure 13-stage (N = 13) signal of fine autocorrelation function, using the GNR {1, 3, 2, 7} with parameters n = 4, S = 13, where k_1 = 1, k_2 = 3, k_3 = 2, k_4 = 7. To see this GNR {1, 3, 2, 7} containing four (n = 4) elements allows an enumeration of all numbers exactly once (λ=1):

1 = 1	4 = 1 + 3	7 = 7	10 = 2 + 7 + 1	13 = 1 + 3 + 2 + 7
2 = 2	5 = 3 + 2	8 = 7 + 1	11 = 7 + 1 + 3	
3 = 3	6 = 1 + 3 + 2	9 = 2 + 7	12 = 3 + 2 + 7	

From equation (10) follows:

$$x_1 = +1, x_2 = -1, x_3 = -1, x_4 = +1, x_5 = -1, x_6 = +1, x_7 = -1, \\ x_8 = -1, x_9 = -1, x_{10} = -1, x_{11} = -1, x_{12} = -1, x_{13} = +1. \tag{11a}$$

Next we regard the GNR {7, 2, 3, 1}, where k_1 = 7, k_2 = 2, k_3 = 3, k_4 = 1.
The GNR {7, 2, 3, 1} containing four (n = 4) elements allows an enumeration of all numbers exactly once (λ=1):

1 = 1	4 = 3 + 1	7 = 7	10 = 1 + 7 + 2	13 =7 + 2 + 3 + 1
2 = 2	5 = 2 + 3	8 = 1 + 7	11 = 3 + 1 + 7	
3 = 3	6 = 2 + 3 + 1	9 = 7 + 2	12 = 7 + 2 + 3	

From equation (10) follows:

$$x_1 = -1, x_2 = -1, x_3 = -1, x_4 = -1, x_5 = -1, x_6 = -1, x_7 = +1, \\ x_8 = -1, x_9 = +1, x_{10} = -1, x_{11} = -1, x_{12} = +1, x_{13} = +1. \tag{11b}$$

For configure 13-stage (N = 13) signal, we can use GNR {1, 3, 2, 7} or GNR {7, 2, 3, 1} as well as any of the GNR with parameters n = 4, S = 13, using underlying reconstruction.

Next we consider optimising coded design by minimax criterion [5, 6]:
Finding the L_{min} $|R_\mu(m)| < L$, m = 1, 2,... N – 1, μ = –1, +1, where

$$R_\mu(m) = \sum_{i=0}^{N-m-1} \mu_i \mu_{i+m} \tag{12}$$

Here is one of solution of the problem using GNR {7, 2, 3, 1). Easy to see that after 5-steps cyclic shift of this code sequence to the left, we obtain:

$$x_1 = -1, x_2 = +1, x_3 = -1, x_4 = -1, x_5 = -1, x_6 = -1, x_7 = +1, \\ x_8 = +1, x_9 = -1, x_{10} = -1, x_{11} = -1, x_{12} = -1, x_{13} = -1. \tag{13}$$

Hence, optimal 13-stage (N = 13) signal of fine autocorrelation function prescribed by minimax criterion based on application of the Gold Numerical Ring with parameters n = 4, S = 13 is constructed.

BIBLIOGRAPHY

[1] Golomb S.W., 1995. Applications of Combinatorial Mathematics to Communication Signal Design. Proc. of the IAM Conf. on Applications of Combinatorial Mathematics, London, U.K.
[2] Robinson J.P., Bernstein A.J., 1967. A class of binary recurrent codes with limited error propagation. IEEE Trans. Inform. Theory. Vol. IT-13, No. 1, pp.106-113.
[3] Atkinson M.D., 1984. Hassenklover: Sets of integers with distinct differences. Sch. Comput. Sci., Carleton Univ., Ottawa, Ont., Canada, Rep SCS-TR-63.
[4] Bandyrska O., Riznyk W., 2008. Systemy pomiarowe o kodach „złotych pierścieni liczbowych". Biuletyn Wojskowej Akademii Technicznej, Vol. LVII, No. 2(650), Warszawa, s. 355-365.
[5] Свердлик М.Б., 1975. Оптимальные дискретные сигналы. М., Сов. радио.
[6] Titsworth R.C., 1963. Optimal and minimax sequences. International Telemetry Conference.

UŻYCIE TEORII SEKWENCJI KOMBINATORYCZNYCH W INNOWACYJNYM KONSTRUOWANIU KODÓW

Streszczenie

Referat dotyczy konstruowania sygnałów o dobrej jakości korelacyjnej lub kodów minimalizowanych według funkcji autokorelacji poprzez jak najlepsze rozmieszczenie kolejności impulsów kodowanych sygnałów w przestrzeni. Opisana metoda bazuje na szczególnych właściwościach pewnych rodzajów struktur kombinatorycznych, zwanych „Złotymi Pierścieniami Liczbowymi" (ZPL), pozwalających uprościć poszukiwanie optymalnych wariantów syntezy takich sygnałów. Metoda konstruowania sygnałów za pomocą ZPL może być z powodzeniem stosowana w energoelektronice, układach sterowania, telekomunikacji i radio-inżynierii.

Słowa kluczowe: sygnał, kod, funkcja autokorelacji, optymalizacja.

UNIWERSYTET TECHNOLOGICZNO-PRZYRODNICZY
IM. JANA I JĘDRZEJA ŚNIADECKICH W BYDGOSZCZY
ZESZYTY NAUKOWE NR 257
ELEKTROTECHNIKA 15 (2010) 53-65

A CONTROL SYSTEM BASED ON THE DC-DC CONVERTER FOR STAND-ALONE VERTICAL-AXIS WIND TURBINES

Ihor Z. Shchur, Oleksandr R. Turlenko

Lvivska Politekhnika National University
Power Engineering and Control Systems Institute
Bandera Str., 12, Lviv-13, 79646, Ukraine
e-mail: i_shchur@yahoo.co.in, turlenko@list.ru

Summary: In this paper the investigation of uncontrollable and adjustable by the boost DC-DC converter systems of autonomous wind turbines are conducted on the basis of computer simulation. To achieve the maximum efficiency of energy transference and conversion at different wind speeds, the optimal combination of regulated and unregulated modes is proposed. The developed control system allows taking off the maximum power from wind without a wind sensor.

Keywords: wind turbine, vertical-axis, wind turbine rotor, PMSG, DC-DC converter, optimal control

1. INTRODUCTION

Energy and environmental crises in which mankind found itself at the turn of the 21st century necessitate increasing use of renewable energy sources, including wind energy. The experience gained over the last two decades in the development of wind power in the world has allowed us to identify two ways of further development: use of powerful (0.1 ... 5 MW) wind turbines (WT) and power stations in industry, and low and medium power (0.3 ... 50 kW) WT for private homes, rural estates, farms etc. Because the latter are meant to work in close proximity to people, in medium to low wind speeds, they must meet high environmental and energy efficiency standards. These standards are best met by the WT with the vertical-axis rotation (VAR) of the wind turbine rotor, which have recently become popular in the world. Compared with traditional wind wheels with the horizontal axis of rotation, the mechanical part of the vertical-axis WT does not require any control, and the transmission can be bearless. However, in order to ensure the high ratio of useful energy from wind power at variable wind speeds, the electromechanical energy conversion systems of VAR WT and electronic control systems must be more complex and multifunctional.

2. ANALYZING THE PROCESSES OF ELECTRICITY GENERATION AND POWER TAKEOFF FROM THE GENERATOR

One of the main elements of the WT is the wind turbine rotor (WTR) which converts wind energy into mechanical energy. Its main parameters are output power P_{WTR} and torque M_{WTR}, which are determined by the following formula [1]:

$$P_{\text{WTR}} = 0.5\rho A C_{\text{P}}(\lambda) V_{\text{w}}^3, \tag{1}$$

$$T_{\text{WTR}} = 0.5\rho A r \frac{C_{\text{P}}(\lambda)}{\lambda} V_{\text{w}}^2, \tag{2}$$

where:

ρ – density of air,

$A = \pi r^2$ – washing area of WTR,

$C_{\text{P}}(\lambda)$ – wind power conversion efficiency factor,

$\lambda = \omega r / V_{\text{w}}$ – tip speed ratio of WT,

ω – angular speed of WTR,

r – WTR radius,

V_{w} – wind speed.

Wind power conversion efficiency factor of WTR depends nonlinearly on its tip speed ratio, and for different turbines there exist different curves which are determined experimentally: for example, by studying the WTR in a wind tunnel. For instance, Fig. 1 showed the dependence $C_{\text{P}}(\lambda)$ for the WTR [1], at the optimal point of which ($\lambda_{\text{opt}} = 3.8$) the maximum of wind power is taken off. Using $C_{\text{P}}(\lambda)$ as expressed in (1) and (2), we can build for a specific WTR the basic dependences that characterize its work, as shown in Fig. 2.

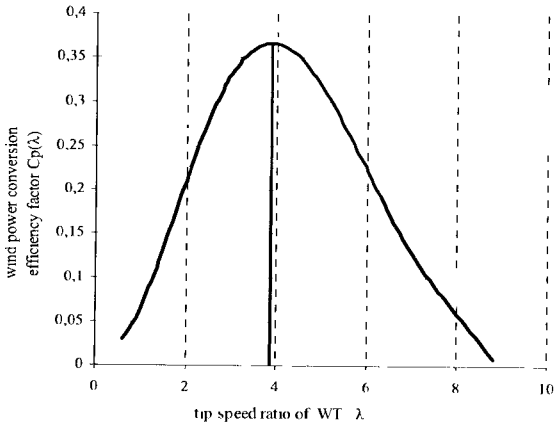

Fig. 1. Wind power conversion efficiency factor of the WTR versus tip speed ratio

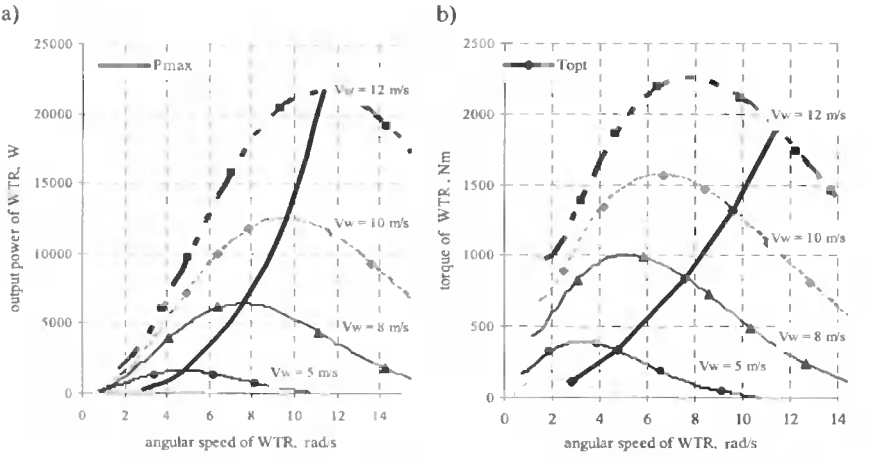

Fig. 2. Dependences of the output parameters of the WTR on its angular speed at different wind speeds: a) power P_{WTR}, b) torque T_{WTR}

To generate electricity, there are various ways of constructing the WT electromechanical systems [2,3]. Asynchronous machines and synchronous machines with electromagnetic excitation are used in the WT that are designed for high wind speeds and operate in parallel to the power networks. Synchronous machines with permanent magnets are more suitable in the WT that are designed for low wind speeds and autonomous load. The use in WT of the multi-pole synchronous generator with permanent magnets (PMSG) allows one to avoid a boost gear (multiplier), which simplifies the design and improves the reliability of WT.

In Eastern Europe, winds of low and medium speed prevail, which makes it a suitable area for the use of low-power WT. In such turbines, especially for turbines with VAR, it is advisable to use the simplest and most reliable system, which is PMSG without a multiplier with a DC link. A number of factors, such as lack of agreement with the electric power companies about connecting the private WT to the power networks, small power of the WT, outages of power and lack of power networks, make it advisable to build autonomous WT that are designed for individual consumers. In such cases, the random character of generation and consumption calls for such element of the WT as the electrochemical battery of accumulators (AB).

There are two main options for taking power from PMSG: uncontrollable – the load of PMSG through passive diode bridge rectifier (DB) directly onto AB, and adjustable – with electronic regulation of the electric load of PMSG (Fig. 3) [4].

The first option (Fig. 3, a) is a simple and more cost-efficient one: for a particular PMSG, one selects the optimum number of AB. However, in this case it is impossible to provide operation in the point of the maximum takeoff of wind power. At low wind speed, the WT hardly generates any electric power, and at large wind speed, it typically overloads AB by charge current, which significantly reduces their life [5].

The second option necessitates the use of a power semiconductor converter: voltage DC-DC converter in the DC link (Fig. 3, b) or an active voltage rectifier (AR) (Fig. 3, c).

In such cases, one can apply a maximum power point tracing (MPPT) system, and one can simultaneously solve other problems of automatic control [5].

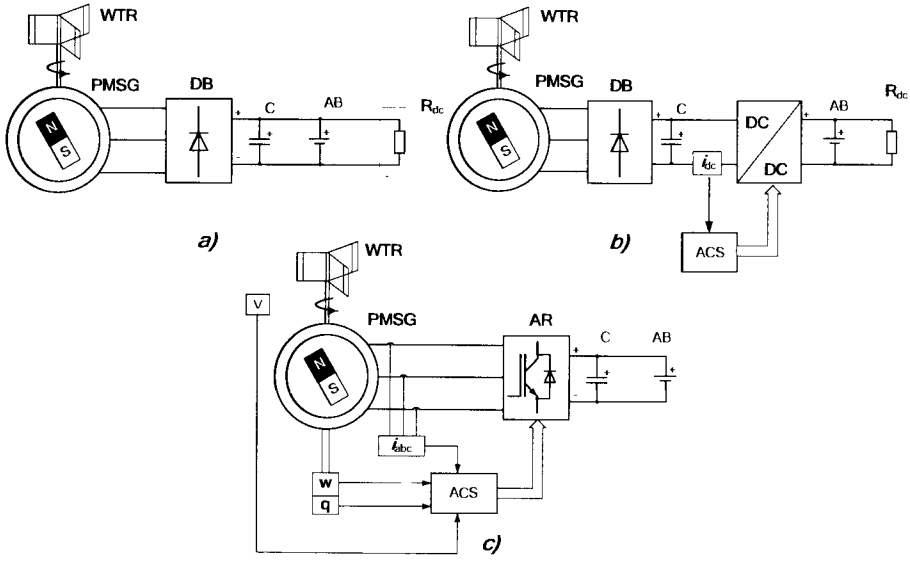

Fig. 3. Functional schemes of taking power from PMSG: a) uncontrollable, b) adjustable with a DC-DC converter; c) adjustable with an active rectifier

In addition to taking into account the peculiarities of low power WT (operation at low wind speeds and for local consumers), one must ensure its highest possible performance at all stages of energy conversion, including taking maximum possible power from the WTR at different wind speeds, transferring the received power to the consumer with minimal losses in all the elements of the power system, and monitoring all the processes. All of these requirements can be best satisfied by the system with AR. However, financial considerations for the low-power WT make it preferable to use a DC-DC converter.

3. COMPUTER SIMULATION OF THE WT: UNCONTROLLABLE AND ADJUSTABLE BY AUTOMATIC CONTROL SYSTEM (ACS) BASED ON THE DC-DC CONVERTER

In order to study the rational parameters of ACS in the first phase of research, it is useful to conduct a computer modeling of the WT with given parameters (see Appendix). It should compare the performance of two configurations of the WT: the conventional one without the automatic control and the one with the DC-DC converter and optimal control (Fig. 3, a, b).

For the simulation of the WT, we used MatLab/Simulink software. The developed computer model (Fig. 4) models the work of the WT and consists of the following subsystems: the WTR, the three-phase PMSG, the diode bridge, the boost DC-DC convert-

er, the AB and the ASC, which allows the MPPT and the charging of the AB at all wind speeds. In this model for the automatic control of the DC-DC converter, we used the optimal linear relationship between wind speed values that were referred in the model, and the angular speed of PMSG. In the case of studying the uncontrollable system, the IGBT transistor in the DC-DC converter did not work.

The control of the IGBT transistor takes place by means of a system that is listed in the subsystem System Control (Fig. 5). It implements the closed system of regulation of the PMSG angular speed with the PID-regulator. Its output voltage is compared with the saw-toothed voltage (carrier frequency 3 kHz), which forms in the subsystem Triangular Generator. The output PWM signal of the comparator controls the gate of the IGBT transistor.

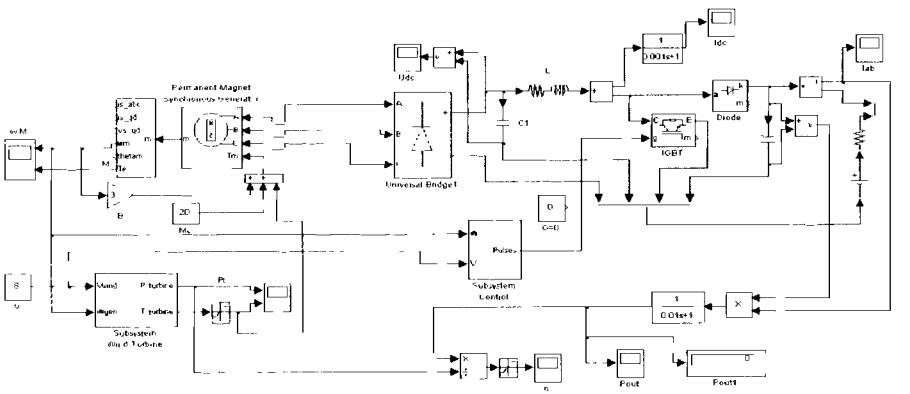

Fig. 4. Basic computer model of the WT with the PMSG and the DC-DC converter

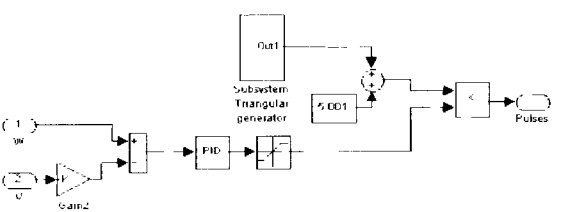

Fig. 5. System Control Subsystem

The energy dependences for both WT systems based on the results of conducted research are given in Fig. 6. Their analysis shows the following:

1. For the uncontrollable WT, the output power value (Fig. 6, a) depends on the number of AB. The nature of the changes in this value with the change of wind speed, and when the amount of AB is constant, does not correspond completely to the character of the maximum power curve shown in Fig. 6, a by the solid line. For the set parameters of the WTR and PMSG, the optimal number of AB is 16, which are connected consistently, when the best match with the maximum power curve is observed. However, electricity generation in this case begins at wind speed of 5 m/s.

2. For the adjustable WT, the output power value (Fig. 6, b) practically does not depend on the number of AB; that is why their number can be selected according to oth-

er criteria. The nature of the changes in this value with the change of wind speed practically corresponds to the nature of the curve of maximum power. Slight deviations from the maximum power curve are observed only at 16 AB and the wind speed of over 10 m/s, when the output voltage of the diode bridge already exceeds the voltage of AB, and the DC/DC converter does not work. Generation of electricity in the regulated WT starts at wind speed of 3 m/s.

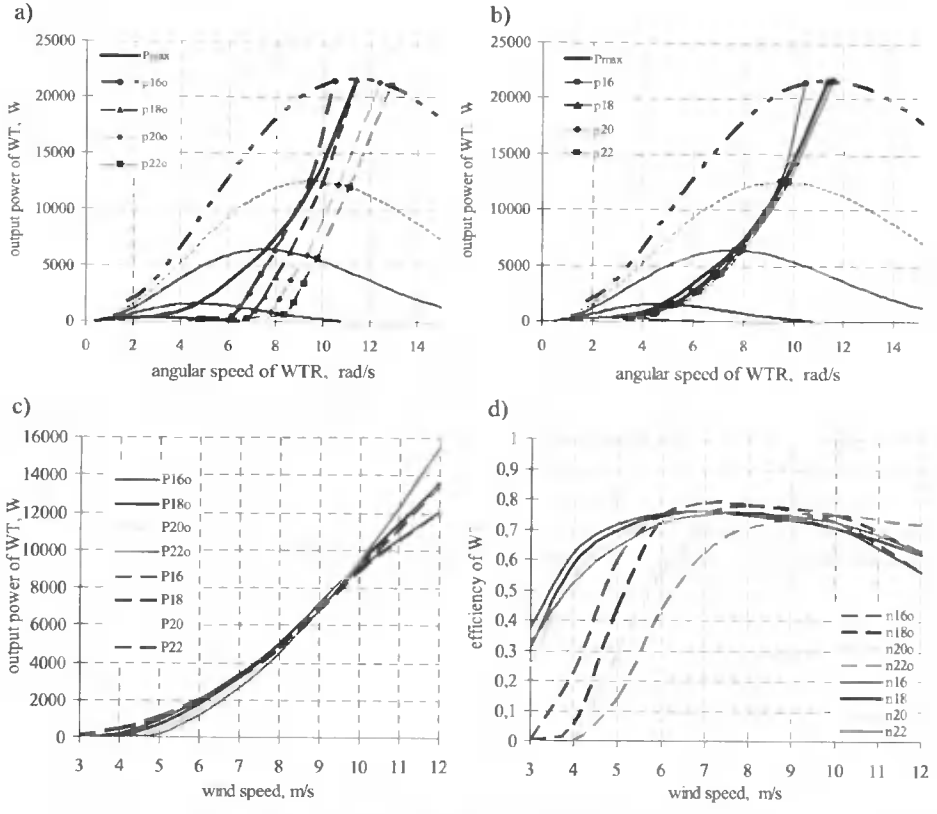

Fig. 6. Energy dependences for uncontrollable and adjustable with the DC-DC converter WT with different numbers of AB (16, 18, 20, 22): a) dependence of the output power of the WT on angular speed at different wind speeds for the unregulated system, b) dependence of the output power of the WT on angular speed at different wind speeds for the adjustable ASC, c) dependence of the output power for unregulated (dotted line) and controlled (solid line) WT systems on wind speed, d) dependence of total efficiency for unregulated (dotted line) and controlled (solid line) WT systems on wind speed

3. Dependences of output power of the WT on wind speed (Fig. 6c) show that for $V_w < 8$ m/s, unregulated electric output power of the WT is significantly lower than the regulated, especially as the number of AB increases. At high wind speeds, $V_w > 8$ m/s, the situation is reversed: the highest electric power output is observed in the unregulated system and at a greater number of the AB. This is because at high output power in the regulated system, switching losses in the DC-DC converter significantly increase. At the

same time, in the unregulated system the output voltage is already high enough to charge AB directly, without significant deviation from the point of maximum power, and at a greater number of AB the same power is transmitted by less current, which helps to reduce resistance losses in the power circuit. This is illustrated well by the dependences of overall efficiency on wind speed, which are defined for all investigated cases and given in Fig. 6d. Total efficiency is defined by

$$\eta_{\Sigma} = \frac{P_{\text{out}}}{P_{\text{WTR.max}}}, \tag{3}$$

where:

P_{out} – output electric power of the WT,

$P_{\text{WTR.max}}$ – maximum power which can be obtained from WTR under a given wind speed (calculated using expression (1) at $C_{\text{P.max}}(\lambda) = 0.37$).

Thus, our study shows that at wind speeds $V_{\text{w}} > 8$ m/s, using the DC/DC converter is impractical. It should work only at low wind speeds, which will always allow operation at the point of maximum power, and the use of low, but lasting wind potential. The power of the DC/DC converter will not exceed one half of the maximum power of the WT. At high wind speeds and high power, the WT system should operate in the unregulated regime, and in order to reduce the total energy losses, one must select the optimum number of AB: in this case, 20, as demonstrated by Fig. 6d.

4. DEVELOPING THE OPTIMAL CONTROL SYSTEM FOR THE TAKEOFF OF WIND ENERGY

In order to provide maximum energy efficiency, the WT should work at the point of maximum output power for each wind speed [1,6]. The key to this is to provide such total electrical and mechanical load of the generator that WTR turns with optimal angular speed at which maximum power is taken from the wind. This corresponds to the optimal points of the tip speed ratio of WTR λ_{opt}, in which the wind power conversion efficiency factor $C_{\text{P}}(\lambda_{\text{opt}})$ reaches a maximum value. Thus, we may formulate the following linear dependence between the optimal value of WTR angular speed ω_{opt} and wind speed V_{w}:

$$\omega_{\text{opt}} = \frac{\lambda_{\text{opt}}}{r} V_{\text{w}}. \tag{4}$$

The condition of WT optimal control (4) is simple and effective, but for its implementation, it is necessary to equip the system with wind speed sensor. In those systems where the wind speed sensor is required in terms of other tasks (for example, in such vertical-axis WT that must be started into operation by preliminary rotation, or in horizontal-axis WT with the electric drive turning of the head to wind orientation), such a simple optimal control system should be used [7,8]. We also used it in previous computer experiments.

Small error in the condition (4) is introduced by a significant increase of power loss in the power part of the WT with the increasing wind speed and the corresponding increase of energy flow. To correct this condition, one should somewhat decrease the generator load, which means to increase slightly the WTR angular speed in comparison with ω_{opt}, defined by (4).

To construct the sensorless optimal control WT systems, a number of ways were developed that differ according to the type of WT (stand-alone, running parallel to the power network), the type of WTR (horizontal or vertical axis, with pitch control of blades), the type of generator (induction or synchronous with modifications), and the principle of their control (scalar or vector), etc. [6-10]. Analysis of different control methods of the WT enabled us to determine the main version of the sensorless optimal control system, which is described in [10] and which works as follows:

As seen from equations (1), (2) and (4), in the optimal point of the WT the following dependences exist between its main parameters:

$$\omega_{opt} = k_{\omega} V_w , \tag{5}$$

$$T_{opt} = k_T V_w^2 , \tag{6}$$

$$P_{max} = k_P V_w^3 , \tag{7}$$

where:

k_{ω}, k_T, k_P are constant coefficients whose values can be easily obtained through the parameters of the WTR from the equations (4), (1) and (2).

Having determined V from the equation (5) and having substituted it in (6), we find the relationship between the optimal values of angular speed and the torque of WTR:

$$T_{opt} = \frac{k_T}{k_{\omega}^2} \omega_{opt}^2 = k_{opt} \omega_{opt}^2 \tag{8}$$

The analysis of the obtained equation (8) and the dependencies $T(\omega)$ at different wind speeds, shown in Fig. 1, allows us to draw the following conclusion: ACS with the control criterion $T^* = k_{opt}\omega^2$, where T^* is the reference value of static load torque of the WTR, which is realized by means of electric load on the generator, will work is stable areas of characteristics and in steady-state will always be approaching the optimal point with maximum power. Thus, for optimal control it is necessary to provide the angular speed sensor of the WTR and to develop the specified ACS.

The first condition is easy to implement since the angular speed can be clearly determined from the frequency of voltage of PMSG.

To implement the second condition, in equation (8) we propose to replace the torque on the proportional to it (nonlinear) value of the load current at DC voltage link I_{DC}, which can be easily measured. To find the monotonous nonlinear dependence $I_{DC.opt} = f(\omega_{opt})$, one can use computer modeling or determine it experimentally in multiple points. For theoretical research, we used the first option and obtained as the results of computer simulation the curve shown in Fig. 7. It is approximated by the following polynomial that is the optimal control law:

$$I^*_{DC.opt} = 16.816 - 10.143 \cdot \omega + 1.909 \cdot \omega^2 - 0.067 \cdot \omega^3 \quad (9)$$

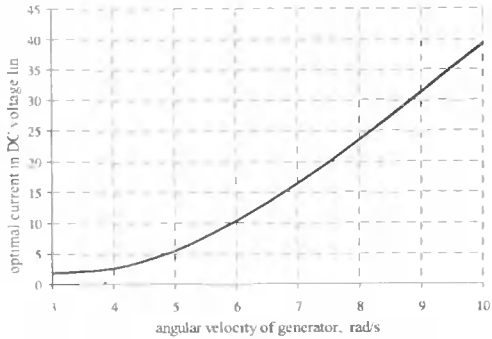

Fig. 7. Relationship between the angular speed of WTR and the current in the DC voltage link at points of optimal work

5. COMPUTER RESEARCH OF THE WORK OF THE WT SENSORLESS ACS

For proposed ACS of the WT, we also developed the computer model on the basis of which we conducted research. This model, unlike previous ones, does not contain a wind sensor, and implements the sensorless optimal control system proposed by us. The reference control signal is the value of current I^*_{DC} in the circuit of generator rectified voltage according to the equation (9). The main model subsystems remained the same as in the case of the model that used the wind sensor (Fig. 4). In this model only subsystem System Control is replaced, the computer model of which is shown in Fig. 8.

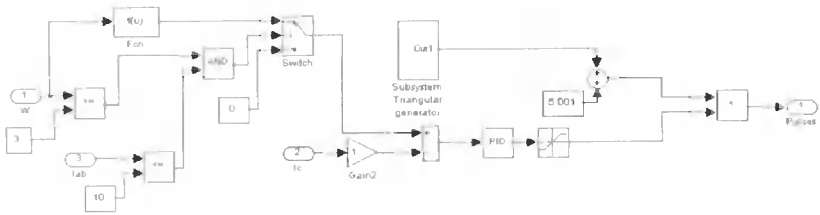

Fig. 8. System Control Subsystem

The value of angular speed ω of PMSG is taken at input of this subsystem, so the block Fcn, which carried dependence (9), forms the reference of current in the DC voltage link. This task may be allowed at input of the current ACS on two conditions: 1) exceeding the minimum angular speed (taken as 3 rad/s) and 2) not exceeding by the rectified generator current of a certain value (for the study done in 10 A), which limits the work range of the DC-DC converter. If both conditions are met, the reference I^*_{DC} is given at the ACS input, where it is compared with the real value of the current in the DC voltage link that comes from a current sensor. The error of current, enhanced by the PID-regulator, comes to the comparator which

compares it to the saw-toothed voltage. Output PWM signal makes it possible to control the opening of the IGBT transistor on a specified range of wind speed.

The received dependences of output electrical power on the angular speed of WTR (Fig. 9a) show how the transition from the regulated mode to the uncontrollable one occurs at the wind speed of 7 m/s. Fig. 9, b shows a similar dependence for the torque of the WTR. These dependences show that the points of best performance for the adopted optimal number (20) of AB appear somewhat to the left of the maximum power curve of the WTR, which, as has been shown above, allows us to take into account the losses in the electrical part of the WT.

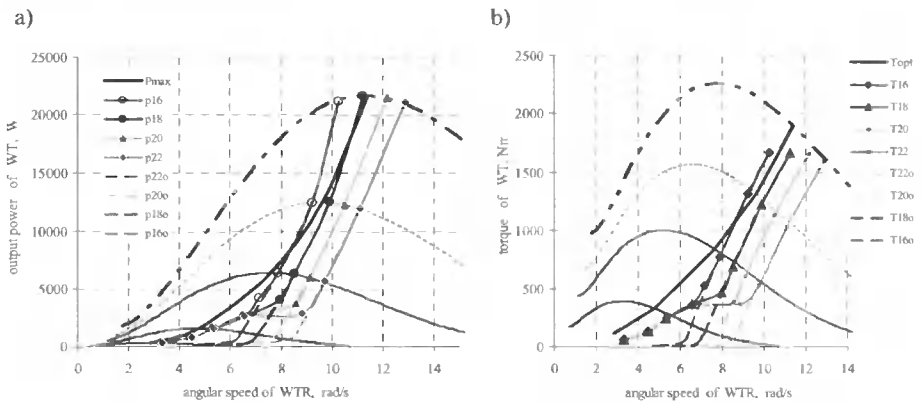

Fig. 9. Energy dependences of the sensorless ACS of the WT for varying numbers (16, 18, 20, 22) of AB: a) output power depends on the angular speed of WTR at different wind speeds; b) torque dependences on the angular speed of WTR at different wind speeds

To study the dynamic modes of the designed WT, the simulation of its work during more than 4 s at variable wind speeds was carried out. To simulation time saving, the total inertia of WTR and PMSG was decreased. The simulated waveform of V_W is given in Fig. 10, a. It also shows how the angular speed w of the WTR with PMSG changes as a result of the WT operation. At the time interval 0-0.4 c V_W is growing to 5 m/s and is kept at this level during 1.5 s. ACS is working this increase of V_W in 0.7 s, changing angular speed w from 0 to steady-state value 5.4 rad/s (optimum value of ω of PMSG for the takeoff of maximum wind power). Then (t = 1.5 s) the second increase of V_W to the value of 10 m/s occurs. At this time interval (0.5 s), one can observe the work of power part of the WT both through the DC-DC convertor (up to ω = 8 rad/s) and directly through the bypass diode (ω > 8 rad/s). When V_W is reduced (t = 2.5 s), the angular speed of the generator decreases, and at ω = 8 rad/s the DC-DC converter turns on (we observe the increase of the falling rate of the generator angular speed). When the steady-state value of wind speed (V_W = 4 m/s) is reached, the ACS ensures the PMSG work in the optimal mode for the maximum takeoff of wind power. Fig. 10, b shows the simulated waveforms of torques on the shaft of WTR T_{WTR} and PMSG T_G, which demonstrate the equality of the latter in the steady state and their differences in the transition. Ripples on the shaft of PMSG arise as a result of non-sinusoidal armature current of the generator, which is caused by its load on the diode bridge with the capacitive output filter. Fig. 10, c shows the simulated waveforms of the output power of the WTR and the WT system and makes it clear that during the growth of the angular speed of the generator,

some part of the WT power goes to the accumulation of the kinetic energy. During the braking in the WT, this kinetic energy is transferred to the output of the WT, which ensures the ratio $\eta = P_{WT}/P_{WTR} > 1$ as seen in Fig. 10, d. The simulated waveform of the output voltage of the diode bridge Uc (Fig. 10, e) clearly shows the work intervals of the DC-DC converter, when Us = 150-230 V and the output voltage is transmitted to AB at 280 V. At the time interval 1.8 - 3 s, the DC-DC converter does not work because the output power is transmitted to the WT output through the bypass diode, which is also evident from the simulated waveforms of the currents, given in Fig. 10, f.

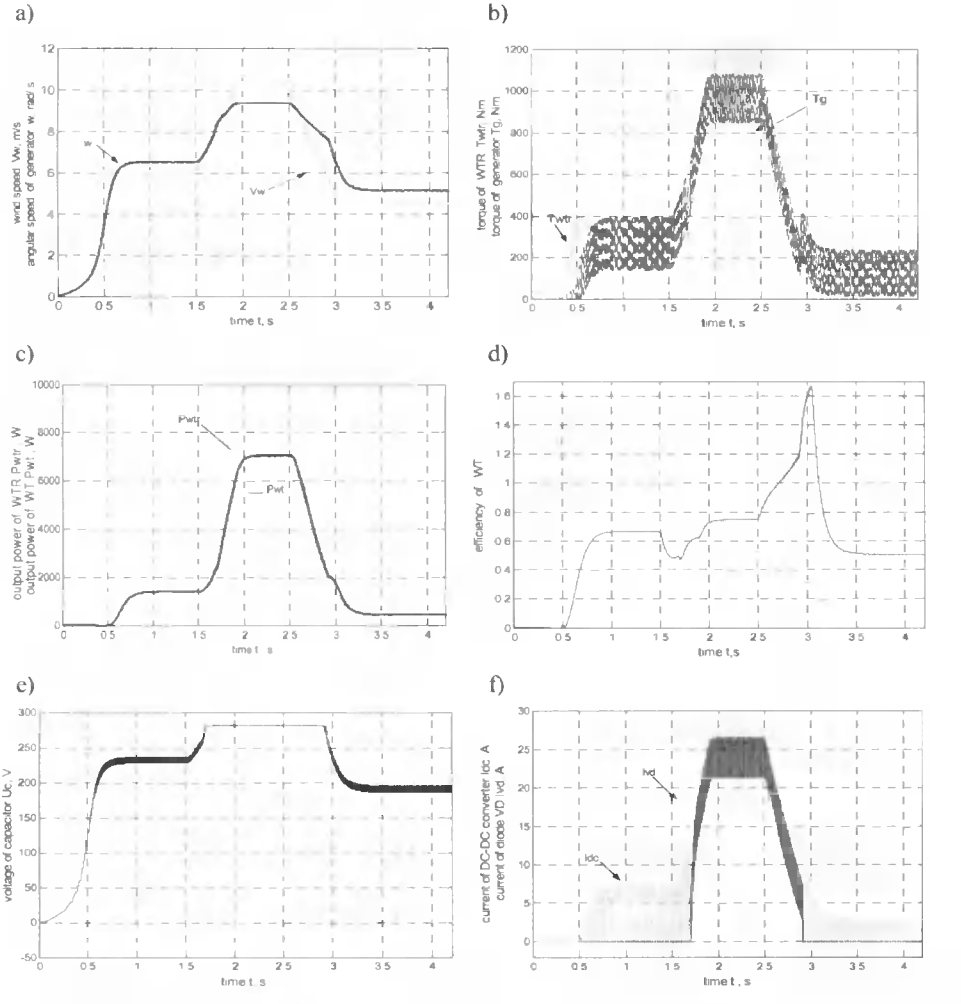

Fig.10. Simulated waveforms of the electrical and mechanical parameters of the sensorless ACS of the WT: a) changes of the wind speed and the generator angular speed during the WT operation; b) torques WTR and PMSG; c) the output power of the WTR and the WT system; d) the ratio of output powers of the WT and the WTR during operation on the test profile of wind speed changes; e) output DC voltage of PMSG; f) the currents of the DC--DC converter Idc and the bypass diode Ivd

6. REALIZATION OF CONTROL SYSTEM

The investigated control system of WT is made as the separate block. It consists of a power part and a microcontroller board. The DC-DC converter is made on the IGBT transistor G4PC50W. The developed control algorithm is implemented in microcontroller ATMEGA 853516PU.

7. CONCLUSIONS

Unregulated takeoff of power from the PMSG is based on the compromise between the capacity of the WT operation at low wind speeds and the prevention of the overload of the AB by charging current at high wind speeds. Using the DC-DC converter for the automatic control of the working point of the WT is advisable only at low power, and later it should work in the unregulated mode with the optimal number of AB. The designed system of optimal control of the WT by changing the parameters of the power part can be adapted to different power of the WT and its type, including both the vertical-axes and the horizontal-axes. The control algorithm incorporated in the microcontroller provides the specific procedure of adjustment for the optimum performance of the WT with unknown parameters. This control system ensures the maximum power of the WT at small and medium wind speeds and the possibility of its operation at great wind speeds without damage to the batteries.

BIBLIOGRAPHY

[1] Bianchi F.D., Battista H.D., Mantz R.J., 2007. Wind Turbine Control Systems: Principles, Modeling and Gain Scheduling Design. London.
[2] Mokin B.I., Mokin O.B., Zukova O. A., 2006. To a question of a choice of wind turbines and electric generators of wind power plants. The bulletin of Vinnitsa polytechnical institute 6, 52-56. (ukr.)
[3] Bernatt J., 2004. Wykorzystanie prądnic synchronicznych do budowy malych elektrowni wiatrowych. Zesz. Probl., Maszyny Elektryczne 68, Katowice, 125-128.
[4] Shchur I.Z., Turlenko O.R., 2009. Power efficiency of different ways of taking off power from the synchronous generator with permanent magnets in wind turbine. The bulletin of Lvivska Politekhnika National University 654, 272-277. (ukr.)
[5] Shchur I.Z., Turlenko O.R., 2008. Many-functional control of an active rectifier in the stand-alone wind turbines with vertical-axis of rotation. The bulletin of Kharkovska Politekhnika National University: Problems of the automated electric drive. The theory and practice 30, 418-420. (ukr.)
[6] Datta R., Ranganathan V.T., 2003. A method of tracking the peak power points for variable speed wind energy conversion system IEEE Trans. on Energy Convers 1(18), 163-168.
[7] Karrari M., Rosehart W., Malik O.P., 2005. Comprehensive control strategy for variable speed cage machine wind generation unit. IEEE Trans. on Energy Convers., Vol. 20, No. 2, 15-423.

[8] Tan K., Islam S., 2004. Optimum control strategies in energy conversion of PMSG wind turbine system without mechanical sensors. IEEE Trans. on Energy Convers., Vol. 19, No. 2, 392-399.
[9] Helle L., Blaabjerg F., 2002. Wind turbine systems Control in Power Electronics, Academic Press, 483-510.
[10] Marimoto S., Nakayama H., Sanada M., 2005. Sensorless output maximization control for variable-speed wind generation system using IPMSG. IEEE Trans. on Ind. Electron., Vol. 41, No. 1, 60-67.

APPENDIX

Nominal parameters of WTR:

$A = 52.96$ m^2; $r = 4.104$ m; $P_{WTR} = 12500$ W for $V_w = 10$ m/s.

Expression $C_p(\lambda)$ for WTR approximated by the following polynomial:

$$C_p(\lambda) = 0.04698 - 0.1285\lambda + 0.196\lambda^2 - 0.05705\lambda^3 + 0.00621\lambda^4 - 0.000236\lambda^5 .$$

Nominal parameters of PMSG:

$P = 10000$ W; $p = 32$ pair of poles;
armature windings: $R = 1$ Ω resistance; $L = 0.005$ H inductance;
$\Phi = 0.7$ Wb magnitude of pole flux;
$J = 10$ kg·m^2 total inertia of WTR and PMSG.

Nominal parameters of each AB:

$U = 12$ V; $C = 200$ Ah.

UKŁAD STEROWANIA DZIAŁAJĄCY W OPARCIU O PRZEKSZTAŁTNIK DC-DC DLA AUTONOMICZNYCH ELEKTROWNI WIATROWYCH Z OSIĄ PIONOWĄ

Streszczenie

W niniejszej pracy są przedstawione wyniki badań układu sterowania autonomicznej elektrowni wiatrowej z osią pionową, który wykorzystuje przekształtnik DC-DC. Badania przeprowadzono za pomocą symulacji komputerowej. Aby osiągnąć maksymalną skuteczność przesyłania i konwersji energii przy różnych prędkościach wiatru zaproponowano optymalną kombinację regulowanych i nieregulowanych trybów pracy. Opracowane sterowanie umożliwia maksymalne wykorzystanie mocy wiatru bez stosowania czujnika prędkości wiatru.

Słowa kluczowe: turbina wiatrowa, pionowa oś, wirnik turbiny wiatrowej, PMSG, DC-DC przekształtnik, sterowanie optymalne

UNIWERSYTET TECHNOLOGICZNO-PRZYRODNICZY
IM. JANA I JĘDRZEJA ŚNIADECKICH W BYDGOSZCZY
ZESZYTY NAUKOWE NR 257
ELEKTROTECHNIKA 15 (2010) 67-74

USING G.652 TELECOMMUNICATION SINGLE-MODE OPTICAL FIBER FOR A MEASUREMENT COIL OF THE INTERFEROMETRIC CURRENT SENSOR

Sławomir Andrzej Torbus

University of Technology and Life Sciences
S. Kaliskiego 7, 85-796 Bydgoszcz
e-mail: slator@utp.edu.pl

Summary: This article describes benefits of using a G.652 telecommunication optical fibre instead of a multi-mode optical fibre for a measurement coil of the interferometric current sensor. The simulation results were presented for coils with various numbers of turns and made of various optical fibres – a single-mode and multi-mode fibre.

Keywords: Verdet constant, mangeto-optical phenomenon, interferometric current sensor, optical fiber current transformer, single-mode optical fiber, multi-mode optical fiber

1. PHYSICAL PRINCIPLES OF INTERFEROMETRIC CURRENT SENSOR OPERATION

The sensor operation is based on an analysis of the properties of a light wave that propagates through the optical fibre and is transformed when subjected to an external magnetic field generated by a live conductor – energy line.

Optical fibres are not optically active when not exposed to an external magnetic field but become active when a magnetic field is applied – the plane of polarization of a light beam is rotated by a certain angle, this is so-called **Faraday effect** (Fig. 1).

This mangeto-optical phenomenon was discovered by Faraday and described with the following formula [1]:

$$\alpha = V \cdot L \cdot B \tag{1}$$

where:

α - the angle of the plane of polarization rotation [rad],

V the Verdet constant (proportionality constant) $\left[\frac{\text{rad}}{\text{T} \cdot \text{m}}\right]$,

L the length of the path where the light and the magnetic field interact [m],

B magnetic flux density $[\text{T}]$.

The Verdet constant in the formula (1) is an empirical value that characterizes the material of the medium as a constant of proportionality between the magnetic excitation and the reaction of glass. Standard types of oxide-based glass – diamagnetic materials have positive and low Verdet constants [1]. Also, as far as diamagnetic materials are concerned, the constant depends to a large extent on the length of a light wave, and to a small extent on the temperature [1].

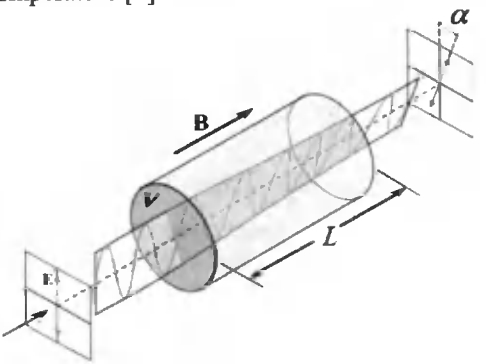

Fig. 1. The influence of an external magnetic field on a change of light polarization [2]

It is possible to describe the relationship between the current in the electric conductor and a change of polarization angle for a single coil of optical fibre with the length of $l = 2 \cdot \pi \cdot R$, where: R – the distance between a fibre coil and the centre of the live conductor (fibre curl radius). In order to do so, the Ampère law must be applied in the integral form:

$$I = \oint_{l=2\cdot\pi R} Hdl = H \cdot l = H \cdot 2 \cdot \pi \cdot R \tag{2}$$

where:

I – current [A],

H – magnetic field strength $\left[\frac{\text{A}}{\text{m}}\right]$.

For a dielectric medium such as a telecommunication fibre, the relationship between the induction and the magnetic field strength may be defined as follows:

$$B = \mu_0 \cdot H \tag{3}$$

where:

$\mu_0 = 4 \cdot \pi \cdot 10^{-7} \left[\frac{\text{V} \cdot \text{s}}{\text{A} \cdot \text{m}}\right]$ – permeability of vacuum

On the basis of the above formulas (2) and (3) the following relationship may be described:

$$B = \frac{\mu_0 \cdot I}{2 \cdot \pi \cdot R} \tag{4}$$

The modification of formula (1) using formula (4) shows that for a sensor fitted with an optical fibre with the length of $L = N \cdot l = N \cdot 2 \cdot \pi \cdot R$ a change of light polarization angle may be described with the following relationship:

$$\alpha = V \cdot \mu_0 \cdot I \cdot N \tag{5}$$

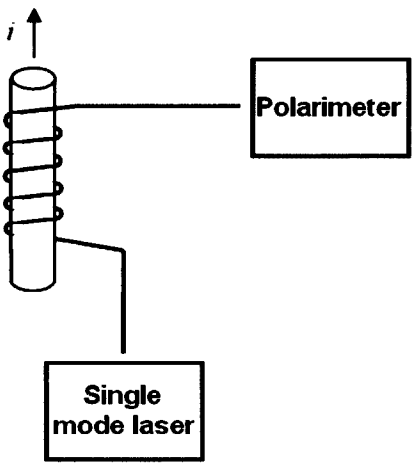

Fig. 2. A block diagram of interferometric fibre sensor

A physical optical waveguide (fibre waveguide, optical fibre) used to construct a measurement coil of the interferometric sensor is made of two layers of silica – SiO_2 that differ in the refractive index. The internal, centrally located layer of glass known as the core is covered by a tightly fitted layer of glass known as the cladding. The core has a higher refractive index – n_1 than the surrounding layer – the cladding with the refractive index – n_2, so that transmission can be carried out on the basis of total internal reflection. Core and cladding diameters of single-mode fibres are standardized. Depending on the type of optical fibre, these are respectively: 5 ÷ 11 μm/125 μm; the diameter of the core of a standard telecommunication fibre is 8 ÷ 9 μm – a standard G.652 step-index profile optical fibre [3]. The standardized diameter of the core of a multi-mode fibre is 50 μm or 62,5 μm, whereas the diameter of cladding is the same as for single-mode fibres – 125 μm.

2. SELECTION OF OPTICAL FIBER FOR A MEASUREMENT COIL OF THR INTERFEROMETRIC CURRENT SENSOR

After determining a polarization angle α with the polarimeter measurement, the equation (5) may be used to determine the current intensity:

$$I = \frac{\alpha}{\mu_0 \cdot V \cdot N} \tag{6}$$

The value of current I (6) is influenced by the Verdet constant V – a parameter characteristic of the type of optical fibre used for the construction of a sensor, and it is described by the Becquerel equation [1]:

$$V = \frac{1}{2} \cdot \frac{e}{m_e} \cdot \frac{\lambda}{c} \cdot \left| \frac{\partial n}{\partial \lambda} \right| \tag{7}$$

where:

$\frac{e}{m_e}$ – specific electronic charge ($1{,}75881962 \cdot 10^{11} \left[\frac{\mathrm{C}}{\mathrm{kg}}\right]$),

λ – wave length [μm],

c – speed of light in vacuum ($c \approx 3 \cdot 10^{8} \left[\frac{\mathrm{m}}{\mathrm{s}}\right]$),

$\left|\frac{\partial n}{\partial \lambda}\right|$ – absolute value of a change of refractive index in relation to wave length $\left[\frac{1}{\mu\mathrm{m}}\right]$.

In the formula (7), $\left|\frac{\partial n}{\partial \lambda}\right|$ is the most interesting element as far as the type optical fibre is concerned, since it describes changes of the refractive index in the core. Those changes may be determined on the basis of the Sellmeier equation [4]:

$$n^2 = 1 + \sum_{i=1}^{3} \frac{a_i \cdot \lambda^2}{\lambda^2 - b_i^2} = 1 + \frac{a_1 \cdot \lambda^2}{\lambda^2 - b_1^2} + \frac{a_2 \cdot \lambda^2}{\lambda^2 - b_2^2} + \frac{a_3 \cdot \lambda^2}{\lambda^2 - b_3^2} \tag{8}$$

where:

a_i, b_i – constants [μm] established empirically for a specific type of glass.

In case of GeO_2 doping, the percentage of the molar concentration of the dope results in an increase of the refractive index in relation to the refractive index of pure glass and therefore the doping is used for the core. The value of indexes a_i and b_i used in the formula (8) for pure silica SiO_2 and for doped silica, depending on the GeO_2 molar concentration are shown in Table 1 [4].

Concentration of GeO_2 dope in the core of standard G.652 telecommunication fibres is approximately 3,1 M%; these are fibres with step-index profile. The concentration of the GeO_2 dope is higher in optical fibres with a more complex refractive index profile (G.653, G.655). The analysis of a multi-mode optical fibre was based on the data from reference sources, namely the Verdet constant for a specific length of a wave [5] ($\lambda = 0{,}63\,\mu\mathrm{m}$, $V = 4{,}6 \cdot 10^{-6} \frac{\mathrm{rad}}{\mathrm{A}} = 3{,}6624 \frac{\mathrm{rad}}{\mathrm{T \cdot m}}$).

Table 1. Indexes a_i and b_i used in the formula (8) [4]

Factors	SiO_2	GeO_2			
		3,1 M%	5,8 M%	7,9 M%	13,5 M%
a_1	0,6961663	0,7028554	0,7088876	0,7136824	0,711040
a_2	0,4079426	0,4146307	0,4206803	0,4254807	0,451885
a_3	0,8974994	0,8974540	0,8956551	0,8964226	0,704048
b_1	0,0684043	0,0727723	0,0609053	0,0617167	0,064270
b_2	0,1162414	0,1143085	0,1254514	0,1270814	0,129408
b_3	9,8961610	9,8961610	9,8961620	9,8961610	9,425478

The value of the derivative relevant for the analysis, following union generalization, has the following form:

$$\frac{\partial n}{\partial \lambda} = -\frac{\sum_{i=1}^{3} \frac{a_i \cdot b_i^2 \cdot \lambda}{\left(\lambda^2 - b_i^2\right)^2}}{\sqrt{1 + \sum_{i=1}^{3} \frac{a_i \cdot \lambda^2}{\lambda^2 - b_i^2}}} \tag{9}$$

where:

a_i, b_i – constants [μm] established empirically for a specific type of glass.

With the derivative of the refractive index in relation to the wavelength (9), its value for a specific wavelength λ may be determined, using data shown in Table 1 for molar concentration GeO_2 at 3,1 M%.

Table 2. Values of the derivative of the refractive index in relation to the wavelength

λ	$\frac{\partial n}{\partial \lambda}$ **for the silicon doping** GeO_2 $\left[\frac{1}{\mu m}\right]$
	3,1 M%
0,63 μm	$-0{,}30286 \cdot 10^{-2}$

Using the formula (7) and results of calculations shown in Table 2, the Verdet constant may be determined depending on the wavelength and the molar concentration of the GeO_2 dope in the core of a single-mode fibre. The calculation results obtained for standard wavelengths used for the transmission in single-mode telecommunication optical fibres are shown in Table 3.

Table 3. Values of the Verdet constant depending on the wavelength and the molar concentration of the GeO_2 dope

λ	V **for the silicon doping** GeO_2 $\left[\frac{\text{rad}}{\text{T}\cdot\text{m}}\right]$
	3,1 M%
0,63 μm	5,5932

Having the parameters of the coil made of a single-mode or multi-mode fibre (sensor) – the number of turns of the coil N, the Verdet constant of the fibre V as well as a measured polarization angle α, it is possible, on the basis of the formula (6), to determine the current in the tested power line. The influence of the above-mentioned parameters of the sensor was determined on the basis of simulations; results of these simulations are presented on diagrams $\alpha = f(I)$.

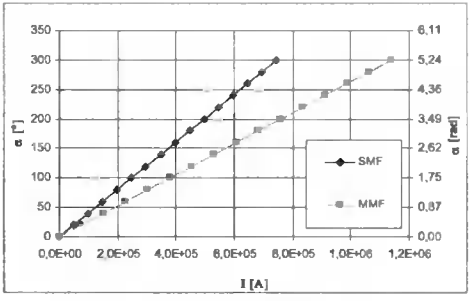

λ = 0,63 μm and N = 1

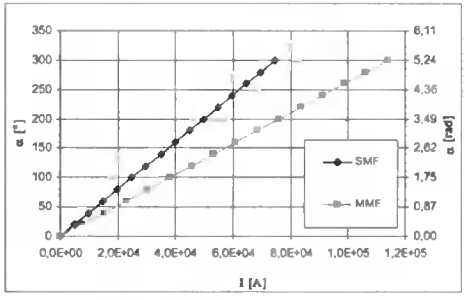

λ = 0,63 μm and N = 10

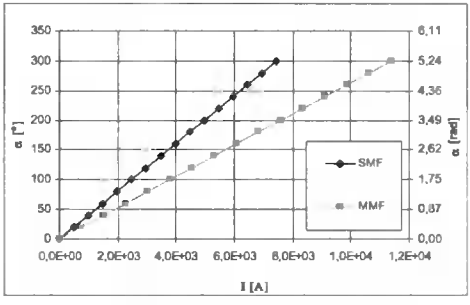

λ = 0,63 μm and N = 100

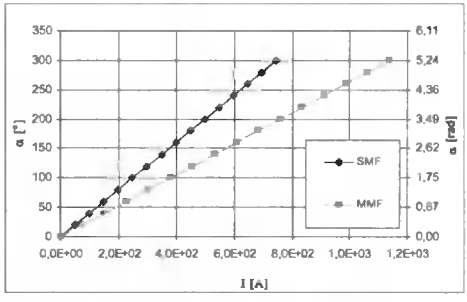

λ = 0,63 μm and N = 1000

Fig. 3. Characteristics $\alpha = f(I)$ depending on optical fibre used and the number of turns of the coil N

6. CONCLUSIONS

The new IEC 61850 standard [6] requires that communication in the power system protection and control and monitoring systems of substations is based on communication protocols that comply with the standard. For that purpose, also current transformers must be fitted with ports that enable digital communication with elements of the power

system protection and the control and monitoring system. Therefore, it is necessary to seek innovative solutions for protection systems characterized by a quick and precise operation, a simple realization and a possibility to locate these systems in individual segments of the power system and even on individual lines. This is fostered by the progress in fibre-optics, in particular the development of optical fibre sensors and measurement transducers. The subject of the interferometric sensor with a measurement coil made of single-mode G.652 fibre is of relevance at the moment.

In conclusion, the following rules for selection of a single-mode optical fibre, in particular a G.652 fibre, to be used in interferometric current sensor may be formulated:

- the sensor design must eliminate macrobendings [7] that could significantly impair measurements. When constructing a measurement coil of the sensor the above-mentioned recommendations related to telecommunication fibres must be followed. For the G.562 optical fibre, it may be assumed that the length of one turn of 23,6 cm will eliminate the influence of macrobendings,
- if the sensor sensitivity is defined as its capability to detect possibly low currents with specified parameters of the sensor (the number of turns of the coil, the wavelength or the angle of polarization rotation), the use of a measurement coil made of a single-mode G.652 fibre instead of a multi-mode fibre will enhance the sensitivity [8],
- the number of turns of the coil influences the sensitivity. Proportionally to the number of coil turns (6) the sensitivity of the sensor increases, regardless of whether or not the measurement coil is made of a G.652 single-mode fibre or a multi-mode fibre. Therefore, very low currents should be measured by sensors with a very high number of coil turns [8].

BIBLIOGRAPHY

[1] Romaniuk R., 2008. Szkło nieliniowe dla fotoniki. Część 5. Szkła Verdeta-Faradaya. Elektronika 10.
[2] http://pl.wikipedia.org/wiki/Zjawisko_Faradaya.
[3] Recommendation ITU - T G.652: Characteristics of a single – mode optical fibre and cable. 03/2003.
[4] Majewski A., 1991. Teoria i projektowanie światłowodów. WNT Warszawa.
[5] Kaczmarek Z., 2006. Światłowodowe czujniki i przetworniki pomiarowe. Agenda wydawnicza PAK Warszawa.
[6] Lizer M., Szweicer W., Wróblewska S., 2010. Elektroniczne przekładniki pomiarowe założenia normy i przegląd rozwiązań technicznych. Automatyka elektroenergetyczna 1.
[7] Ratuszek M., 2002. Analiza pomiarów reflektometrycznych sieci światłowodowych dla poszerzonego zakresu długości fal pomiarowych λ = 1310, 1410, 1450, 1550, 1625 nm. Krajowe Symp. Telekomunikacji, Bydgoszcz.
[8] Torbus S.A., Ratuszek M., 2010. The selection method of the single mode telecommunication fiber to the interferometric current sensor depending on the destination areas. SPIE, Wilga.

ZASTOSOWANIE JEDNOMODOWEGO ŚWIATŁOWODU TELEKOMUNIKACYJNEGO G.652 DO REALIZACJI CEWKI POMIAROWEJ W INTERFEROMETRYCZNYM CZUJNIKU NATĘŻENIA PRĄDU

Streszczenie

W artykule pokazano, że preferowane jest stosowanie standardowego światłowodu telekomunikacyjnego G.652 do wykonania cewki pomiarowej interferometrycznego czujnika natężenia prądu, zamiast światłowodu wielomodowego. Przedstawiono wyniki symulacji dla cewek o różnej liczbie zwojów i różnych wartości natężenia prądu dla dwóch różnych typów włókien światłowodowych – jednomodowego i wielomodowego.

Słowa kluczowe: stała Verdeta, zjawisko magnetooptyczne Faradaya, interferometryczny czujnik natężenia prądu, światłowodowy przekładnik prądowy, światłowód jednomodowy, światłowód wielomodowy

ISSN 0209-0570